

The Origin of the Galaxy Mass-Metallicity Relation and Implications for Galactic Outflows

Kristian Finlator & Romeel Davé

Astronomy Department, University of Arizona, Tucson, AZ 85721

3 September 2021

ABSTRACT

Using cosmological hydrodynamic simulations that dynamically incorporate enriched galactic outflows together with analytical modeling, we study the origin of the stellar mass–gas-phase metallicity relation (MZR). We find that metallicities are driven by an equilibrium between the rate of enrichment owing to star formation and the rate of dilution owing to infall of unenriched gas. This equilibrium is in turn governed by the outflow strength. As such, the MZR provides valuable insights and strong constraints on galactic outflow properties across cosmic time. We compare three outflow models: No outflows, a “constant wind” model that emulates the popular Dekel & Silk (1986) scenario, and a “momentum-driven wind” model that best reproduces $z \gtrsim 2$ intergalactic medium metallicity data (Oppenheimer & Davé 2006). Only the momentum-driven wind scaling simulation is able to reproduce the observed $z \sim 2$ MZR’s slope, amplitude, and scatter. In order to understand why, we construct a one-zone chemical evolution model guided by simulations. This model shows that the MZR in our outflow simulations can be understood in terms of three parameters: (1) The *equilibrium metallicity* $Z_{g,\text{eq}} = y\dot{M}_{\text{SFR}}/\dot{M}_{\text{ACC}}$ (where y =net yield), reflecting the enrichment balance between star formation rate \dot{M}_{SFR} and gas accretion rate \dot{M}_{ACC} ; (2) the *dilution time* $t_d = M_g/\dot{M}_{\text{ACC}}$, representing the timescale for a galaxy to return to $Z_{g,\text{eq}}$ after a metallicity-perturbing interaction; and (3) the *blowout mass* M_{blowout} , which is the galaxy stellar mass above which winds can escape its halo. Without outflows, galaxy metallicities exceed observations by $\sim \times 2 - 3$, although the slope of the MZR is roughly correct owing to greater star formation efficiencies in larger galaxies. When outflows with mass loading factor η_W are present, galaxies below M_{blowout} obey $Z_{g,\text{eq}} \approx y/(1 + \eta_W)$, while above M_{blowout} , $Z_{g,\text{eq}} \rightarrow y$. Our constant wind model has $M_{\text{blowout}} \sim 10^{10} M_\odot$, which yields a sharp upturn in the MZR above this scale and a flat MZR with large scatter below it, in strong disagreement with observations. Our momentum-driven wind model naturally reproduces the observed $Z_g \propto M_*^{0.3}$ because $Z_{g,\text{eq}} \propto \eta_W^{-1} \propto M_*^{1/3}$ when $\eta_W \gg 1$ (i.e. at low masses). The flattening of the MZR at $M_* \gtrsim 10^{10.5} M_\odot$ observed by Tremonti et al. (2004) is reflective of the mass scale where $\eta_W \sim 1$, rather than a characteristic outflow speed; in fact, the outflow speed plays little role in the MZR except through M_{blowout} . The tight observed MZR scatter is ensured when $t_d \lesssim$ dynamical time, which is only satisfied at all masses in our momentum-driven wind model. We also discuss secondary effects on the MZR, such as baryonic stripping from neighboring galaxies’ outflows.

Key words: cosmology: theory — galaxies: abundances — galaxies: evolution

1 INTRODUCTION

In the reigning hierarchical model of galaxy formation, cooling times for moderate overdensity gas at high redshifts ($z > 3$) are shorter than a Hubble time, and protogalaxies accrete gas from the intergalactic medium (IGM) at rates that increase with time (e.g., Birnboim et al. 2007).

Gas forms into stars at rates that mainly track the rising gas accretion rates (Kereš et al. 2005); these rates also scale with galaxy mass and are occasionally boosted by mergers (e.g. Somerville et al. 2001; Straughn et al. 2006). Each generation of stars in turn enriches the surrounding gas with heavy elements. The young galaxies also drive much of their enriched gas out via galactic superwinds, lac-

ing the IGM with heavy elements (Adelberger et al. 2005b, 2003; Schaerer 2003) while suppressing their own star formation (Springel & Hernquist 2003b; Oppenheimer & Davé 2006). As the universe expands further, cooling times rise, until $z \sim 1 - 2$ when the cooling time at moderate overdensities exceeds the Hubble time, and gas accretion rates and star formation rates begin to decline.

At any given epoch the accumulated history of star formation, inflows, and outflows affects a galaxy’s mass and its metallicity. Hence one expects these quantities (or their proxies) to be correlated in some way, and furthermore for this correlation to encode information about the physical processes that govern galaxy formation. In this paper, we investigate what constraints may be placed on such processes, particularly outflow processes that are currently the most poorly understood, based on the observed mass-metallicity relation (MZR) of galaxies.

McClure & van den Bergh (1968) were the first to observe a correlation between the luminosity and metallicity of elliptical galaxies, and Lequeux et al. (1979) were the first to show that total mass (or, equivalently, rotational velocity) correlates with metallicity for irregular and blue compact galaxies. The question of which relationship is more fundamental (Zaritsky et al. 1994; Garnett et al. 1997) was resolved when Tremonti et al. (2004) showed, for a sample of $\approx 53,000$ star-forming galaxies from the Sloan Digital Sky Survey, that the MZR possesses much less intrinsic scatter than the luminosity-metallicity relation. The trends seen by Tremonti et al. (2004) have recently been shown to extend unbroken to much lower masses by Lee et al. (2006), confirming the idea (Garnett 2002) that a single mechanism may govern galaxies’ metallicities across five decades in stellar mass. Finally, the MZR is observed to evolve slowly such that galaxies of a given stellar mass are only moderately more enriched today as compared to in the early Universe (Shapley et al. 2005; Savaglio et al. 2005; Erb et al. 2006; Berger et al. 2006).

A number of mechanisms have been proposed to explain the observed trends. Building upon an idea originally introduced by Mathews & Baker (1971) and Larson (1974), Dekel & Silk (1986) and Dekel & Woo (2003) showed that supernova feedback energy could give rise to a range of observed trends in low mass galaxies including the MZR, if the supernova energy injected into galaxies’ interstellar media is proportional to its stellar mass (as one might naïvely expect). In this model, there is a characteristic halo circular velocity of $\sim 100 \text{ km s}^{-1}$ above which galaxies retain their gas, and below which gas removal becomes progressively more efficient.

More recent investigations have attempted to put the MZR in a hierarchical context. De Lucia et al. (2004) used semianalytical models to suggest that such winds can be tuned to reproduce the $z \approx 0$ MZR irrespective of what the outflows do upon leaving the galaxy. De Rossi et al. (2006) and Tassis et al. (2006) used cosmological hydrodynamic simulations without strong supernova feedback to obtain rough agreement with the Tremonti et al. (2004) and Dekel & Woo (2003) MZRs, respectively. Both works cite the possible role of a varying star formation efficiency with stellar mass, while Tassis et al. (2006) also suggest that the observed low effective yields in low-mass galaxies could result from mixing processes that transport metals

to galaxies’ outer disks, where they are difficult to observe. Brooks et al. (2006) used cosmological hydrodynamic simulations with a treatment for pressure-driven outflows to argue that mass loss does not directly suppress the metallicities of low mass galaxies, and instead argued that supernova feedback leads to low star formation efficiencies in low-mass galaxies, which in turn lead to low metallicities; it is particularly encouraging that their model reproduces the observed trends both at $z \sim 2$ and at $z \sim 0$. Kobayashi et al. (2007) used a similar model that also incorporated a treatment for hypernova feedback and obtained qualitative agreement with the same observations. However, they concluded that their MZR is primarily driven by a tendency for low-mass galaxies to eject relatively more material in outflows, an idea that our results support. A more speculative idea from Köppen et al. (2006) suggests that the observed trends at low redshift can be reproduced by postulating that the stellar initial mass function (IMF) is more top-heavy in galaxies with higher star formation rates, thereby producing higher metal yields.

In short, the galaxy MZR has been speculated as arising from variation in mass loss, star formation efficiency, and/or yield with galaxy stellar mass. A key aim of this present work is to distinguish between these alternatives, and determine the key driver that sets the MZR.

A feature that has garnered much attention is the apparent flattening of the MZR for $M_* \gtrsim 10^{10.5} M_\odot$. This characteristic mass also seems to divide galaxy properties in general, such as blue from red and high surface brightness from low (Kauffmann et al. 2004). Dekel & Woo (2003) note that their predicted characteristic halo velocity (Dekel & Silk 1986) is in broad agreement with this mass. Building on this, Tremonti et al. (2004) and Garnett (2002) proposed that winds may not be effective at driving metals out of galaxies above this mass range (see however Dalcanton 2006). One physical model that could give rise to this behavior is the “constant wind” scenario. In this model, the low effective yields observed in small galaxies result from winds that have roughly constant velocities at all masses, and hence are progressively more effective at driving out metals from the shallower potential wells of smaller galaxies. Consequently, the escape velocity at the observed MZR turnover should be an indicator of the characteristic wind speed. At present, this scenario of mass loss variation is probably the most widely accepted explanation for the MZR’s shape.

In this work we show that such a constant wind scenario, when incorporated into a fully three-dimensional hierarchical structure formation simulation, produces an MZR shape that is in poor agreement with observations, for reasons that can be understood from straightforward physical arguments. This scenario has been also called into question recently by observational analyses of dwarf galaxy metallicities. Lee et al. (2006) note that such energetic speeds from small galaxies should produce a much greater scatter in metallicities than observed in their sample of dwarf irregulars. They instead propose that “a less energetic form of metal-enhanced mass loss than blowouts could explain the small scatter.” Dalcanton (2006) used a rigorous treatment of the effects of outflows to show that outflows alone cannot account for the low observed effective yields of dwarf galaxies, unless the winds are substantially enriched relative to ISM gas. She proposed instead that the low gas surface den-

sities of galaxies with circular velocities below 120 km s^{-1} lead to low star formation rates (SFRs) so that their effective yields “recover” from outflows relatively slowly. Hence she suggests star formation efficiency variations are the key driver of the MZR. The results we present here are generally in agreement with this conclusion.

In this paper we use cosmological hydrodynamic simulations and simple analytical models to investigate the origin of the mass-metallicity relation. Our simulations employ parameterized outflows from star-forming galaxies that drive metals into the IGM, and hence we directly track the growth of galaxy metallicity along with its mass within a full three-dimensional hierarchical structure formation scenario. In Oppenheimer & Davé (2006) we introduced our outflow models, and showed in particular that models in which the outflow velocity scaled linearly with galaxy circular velocity while the mass loading factor (i.e. the rate of mass ejection relative to the star formation rate) scaled inversely with it were remarkably successful at enriching the IGM to observed levels at $z \sim 2 - 6$. These scalings arise naturally for radiation or momentum-driven winds (e.g. Murray, Quatert, & Thompson 2005), though for our purposes the important aspect is the scaling relations themselves and not the physical mechanism responsible. Interestingly, recent observations of local galactic outflows indicate momentum-driven wind scalings (Martin 2005; Rupke et al. 2005), providing an intriguing connection between rare local outflows and the more ubiquitous and generally stronger outflows at $z \gtrsim 2$.

In our preliminary study of the MZR (Davé et al. 2006b), we compared various outflow models with the $z \sim 2$ MZR seen by Erb et al. (2006) and examined its evolution from $z = 6 \rightarrow 2$. We found that the “constant wind” model as implemented by Springel & Hernquist (2003b) leads to poor agreement with observations at $z \sim 2$, while our momentum-driven wind scalings naturally reproduce the slope and amplitude of the observed relation. While this work provided independent support for the outflow model concurrently favored by IGM metallicity data, it did little to address the fundamental question of what physical processes govern the MZR’s slope, amplitude, scatter, and evolution.

In order to improve our understanding of the relationship between outflows and the MZR, we follow a trajectory that encompasses three basic goals:

(1) *Show that our numerical model reproduces observations at $z \sim 2$.* In this step we describe our simulations (Section 2) and discuss the mass scales that our outflow models introduce. Next we compare the simulated MZRs assuming different outflow models with the observed MZR at $z = 2$ (Section 3). Our finding that momentum-driven outflows produce the best agreement with observations motivates a more detailed investigation into the origin of the MZR within our simulations.

(2) *“Boil down” our numerical model to a set of key processes and combine them in an analytically tractable way.* We begin this step by introducing a simple model that captures the main processes that impact the growth of galaxies’ stellar masses and metallicities (Section 4). Next, we investigate how gas accretion and star formation rates vary with mass and time in each outflow scenario in order to treat them accurately in our analytical model. We continue this discussion in Section 5 with a detailed investigation into the

Table 1. Simulation parameters

L^a	ϵ^b	m_{SPH}^c	m_{dark}^c	$M_{*,\text{min}}^{c,d}$	z_{end}^e
16	1.25	3.87	25.2	248	$2,0^e$
32	2.5	31.0	201	1984	$2,0^e$

^aBox length of cubic volume, in comoving $h^{-1}\text{Mpc}$.

^bEquivalent Plummer gravitational softening length, in comoving $h^{-1}\text{kpc}$.

^cAll masses quoted in units of $10^6 M_{\odot}$.

^dMinimum resolved galaxy stellar mass.

^eFirst number for nw, cw runs; second for vzw.

time-integrated effects of outflows on our simulated galaxies at $z = 2$. In Section 6 we trace the observable trends at $z = 2$ back in time in order to understand how galaxies evolve through the MZR. In Section 6.3 we verify that our analytical model reproduces this evolution reasonably well, which suggests that our analytical model accounts for the important processes that drive the observable MZR.

(3) *Use the analytical model to determine what drives the observable MZR in the presence of outflows.* In Section 7 we use our analytical model to determine what drives the form of the observable MZR; the reader may wish to skip directly to this Section for a relatively self-contained explanation of the origin of the MZR. Here we show why our momentum-driven wind model is successful at reproducing the $z \approx 2$ MZR, and why other models are not. More generally, we show how the observed MZR’s slope, amplitude, and scatter down to low masses provide stringent constraints on outflow models.

Finally, in Section 8 we present our conclusions.

2 SIMULATIONS

2.1 Simulations and Sample Definition

We employ the parallel cosmological galaxy formation code Gadget-2 (Springel & Hernquist 2002) in this study. This code uses an entropy-conservative formulation of smoothed particle hydrodynamics (SPH) along with a tree-particle-mesh algorithm for handling gravity. Heating is included via a spatially uniform photoionizing background (Haardt & Madau 2001). Gas particles undergo radiative cooling under the assumption of ionization equilibrium, where we account for metal-line cooling using the collisional ionization equilibrium tables of Sutherland & Dopita (1993). The metal cooling function is interpolated to the gas metallicity as tracked self-consistently by Gadget-2 (for details see Oppenheimer & Davé 2006). Stars are formed from dense gas via a subresolution multi-phase model that tracks condensation and evaporation in the interstellar medium following McKee & Ostriker (1977). The model is tuned via a single parameter, the star formation timescale, to reproduce the Kennicutt (1998) relation; see Springel & Hernquist (2003a) for details. Star-forming gas continually self-enriches

under an instantaneous recycling approximation. The effects of Type Ia supernovae are neglected; this should not affect comparisons with observed Oxygen abundances. In reality Type II supernovae occur with a time delay of 10–30 Myr, longer than our typical timestep of \sim a few Myr, hence the assumption of instantaneous feedback is inappropriate if gas accretion or star formation is believed to vary on shorter timescales. However, our simulations (and observations; Noeske et al. 2007) indicate that star formation occurs in a predominantly smooth fashion, hence instantaneous feedback is unlikely to introduce significant errors. Delayed feedback from low-mass stars is also neglected. When star particles are spawned (in two stages, each with half the original gas particle’s mass), they inherit the metallicity of the parent gas particle and from then on cannot be further enriched.

We model galactic outflows using a Monte Carlo approach. First we define the wind model by two parameters: a wind speed V_W and a mass loading factor η_W , which is the ratio of the outflow mass rate to the star formation rate. These parameters can be chosen to be constant or scale with galaxy properties. During the simulation run, for each star-forming particle we compute a probability that it enters into an outflow based on its star formation rate and η_W , and use a random number to decide whether that particle will enter into an outflow. If so, we kick it with a velocity of V_W in the direction of $\mathbf{v} \times \mathbf{a}$, which would be purely unipolar for a thin disk but more typically has a large opening angle of $\sim 45^\circ$. The hydrodynamic forces are turned off for that wind particle until it reaches a density of one-tenth the critical density for star formation, or else it travels for a time greater than $(20 \text{ kpc/h})/V_W$. The outflow particle carries its own metals out of the galaxy; it is not preferentially enriched.

In order to explore the effects of superwind feedback on the MZR, we concentrate on three outflow schemes: A no-wind (nw) model, a “constant wind” (cw) model where $V_W = 484 \text{ km s}^{-1}$ and $\eta_W = 2$ (this is the scheme used in the runs of Springel & Hernquist 2003b), and a “momentum-driven wind” (vzw) model where $V_W \propto \sigma$ and $\eta = (300 \text{ km s}^{-1})/\sigma$, where the velocity dispersion σ is estimated from the local gravitational potential. The exact scalings are taken from the momentum-driven wind model of Murray, Quatert, & Thompson (2005); see Oppenheimer & Davé (2006) for details. The vzw model also gives a velocity boost in low-metallicity systems, based on the arguments that more UV photons are produced per unit stellar mass at lower metallicities (specifically, we employ eqn. 1 of Schaerer 2003), and that it is these UV photons that are driving the wind (Murray, Quatert, & Thompson 2005). Using larger simulations evolved to low redshift, we have verified that both models broadly reproduce the star formation history of the universe (Oppenheimer & Davé 2006, Figure 4); this constrains the choice of parameter values.

We run a total of six simulations: two different volumes, each with our three different superwind schemes, as detailed in Table 1. All runs assume a WMAP-concordant cosmology (Spergel et al. 2003) having $\Omega = 0.3$, $\Lambda = 0.7$, $H_0 = 70 \text{ km s}^{-1} \text{ Mpc}^{-1}$, $\sigma_8 = 0.9$, and $\Omega_b = 0.04$. Each run has 256^3 dark matter and 256^3 gas particles, evolved from well in the linear regime.

We identify galaxies using Spline Kernel Interpolative DENMAX and dark matter halos using the spherical over-

density algorithm (see Kereš et al. 2005, for full descriptions). In previous papers we have shown that imposing a mass resolution cut of 64 star particles leads to a converged sample in terms of stellar mass and star formation history (Finlator et al. 2006, 2007; Davé et al. 2006a). In the present work we make an even more conservative cut at 128 star particles in order to study the scatter in our simulated trends. Hence our minimum resolved galaxy stellar mass ranges from $2.5 \times 10^8 M_\odot$ in our higher-resolution $16h^{-1} \text{ Mpc}$ runs to $2.0 \times 10^9 M_\odot$ in our larger volume $32h^{-1} \text{ Mpc}$ runs. Just as we did in Davé et al. (2006a), we will often show both runs on the same plot, and the smoothness of trends in overlapping mass ranges is to be noted as an indicator of numerical resolution convergence. We have also run higher-resolution simulations in $8h^{-1} \text{ Mpc}$ volumes and confirmed that the trends that we identify continue to lower masses, though the galaxies in these runs are unobservably small at the redshifts where we will perform comparisons to data.

2.2 Scales in the Wind Models

Our wind models introduce several mass scales that are important in understanding the behavior of the MZR. The *reheating scale* is the scale below which galaxies produce enough supernova energy to unbind all of their gas. The *blowout scale* is the scale below which the wind speed exceeds the escape velocity of the halo. Here we compute values for these scales in our wind models.

We first consider the reheating scale in the cw model. The virial energy of the baryons in a halo scales with the halo mass as $E_{\text{vir}} \propto M^{5/3}$ whereas the feedback energy scales as $E_{\text{wind}} \propto M$ (assuming that the fraction of baryons converted to stars f_* varies slowly with M). The ratio of these energies thus scales as $E_{\text{wind}}/E_{\text{vir}} \propto M^{-2/3}$ with the implication that the relative importance of wind heating declines as mass increases in the cw model. Below the “reheating scale”, a galaxy’s winds produce enough energy to expel all of the baryons from the halo; this is analogous to the critical scale for supernova-driven mass loss proposed by Dekel & Silk (1986). In the spherical collapse scenario (e.g., Dekel & Woo 2003) it can be shown that this scale corresponds to a stellar mass of

$$\begin{aligned} M_* &= \frac{f_*^{5/2} \eta_W^{3/2} V_W^3}{2^{3/2} G^{3/2}} \frac{\Omega_b}{\Omega_m} \left[\frac{4\pi}{3} \Delta(z) \rho(z) \right]^{-1/2} \\ &= \frac{4 \times 10^{10} M_\odot}{(1+z)^{3/2}} \left(\frac{f_*}{0.1} \right)^{5/2} \left(\frac{\eta_W}{2} \right)^{3/2} \left(\frac{V_W}{484 \text{ km s}^{-1}} \right)^3 \end{aligned} \quad (1)$$

or a halo circular velocity of

$$\begin{aligned} V &= V_W \left(\frac{f_* \eta_W}{2} \right)^{1/2} \\ &= 150 \text{ km s}^{-1} \left(\frac{V_W}{484 \text{ km s}^{-1}} \right) \left(\frac{f_* \eta_W}{0.1 \cdot 2} \right)^{1/2}. \end{aligned} \quad (3)$$

Here, $\Delta(z) \approx 200$ is the overdensity of collapsed structures, which varies weakly with redshift (Dekel & Woo 2003); η_W is the mass loading factor of the winds; and V_W is the wind speed. Note that the circular velocity of the reheating scale in the cw model is similar to the critical velocity identified by Dekel & Silk (1986). This is expected because the energy injected by winds assuming these parameters is comparable to the supernova feedback energy (Springel & Hernquist

2003b). Hence a comparison between our cw model and observations constitutes a quantitative test of the Dekel & Silk (1986) scenario.

In galaxies above the blowout scale, our constant wind model outflows should escape from the galaxies' halos provided that they couple inefficiently with the ambient halo gas. Under reasonable assumptions regarding the depth of the galaxy's potential well, the ratio of the escape velocity to the halo circular velocity lies within the range $V_{\text{esc}}/V \approx 1.5\text{--}3.5$ (e.g., Martin 1999). In the spherical collapse model, the blowout scale in the cw model is therefore given by

$$M_* = \frac{f_* V_W^3 (V/V_{\text{esc}})^3 \Omega_b}{G^{3/2} \Omega_m} \left[\frac{4\pi}{3} \Delta(z) \rho(z) \right]^{-1/2} \quad (5)$$

$$= \frac{6 \times 10^{10} M_\odot}{(1+z)^{3/2}} \left(\frac{f_*}{0.1} \right) \left(\frac{V_W}{484 \text{ km s}^{-1}} \frac{V/V_{\text{esc}}}{0.4} \right)^3 \quad (6)$$

Both the reheating scale and the blowout scale fall within the range that is resolved by our simulations, hence we expect to see features in the MZR indicating that the two effects grow significantly more effective below this scale and decreasingly effective above it. In Section 5.1 we will show that this is indeed what happens, although we will argue that blowout is much more important than reheating in our models. In Section 7 we will use simple physical arguments to show how the existence of a blowout scale leads to predictions that conflict with observations.

In the vzw model, $\eta_W = \sigma_0/\sigma$ and $V_W = k\sigma$, where σ_0 is a constant, σ is the halo velocity dispersion, and k relates the wind velocity and the halo velocity dispersion to the ratio of the galaxy luminosity to the galactic Eddington luminosity (Murray, Quatert, & Thompson 2005); $k = 6.7$ on average. Hence by construction, all galaxies are above the blowout scale in this model. With these assumptions, the injected energy scales as $E_{\text{wind}} \propto M \eta_W \sigma^2 \propto \sigma^4 \propto M^{4/3}$, and the ratio of the heating energy to the virial energy scales as $E_{\text{wind}}/E_{\text{vir}} \propto M^{-1/3}$ —more shallowly than in the cw model. In this case, the reheating scale is given by

$$M_* = \frac{k^6 \sigma_0^3 f_*^4}{8G^{3/2}} \left(\frac{\Omega_b}{\Omega_m} \right) \left(\frac{4\pi}{3} \Delta(z) \rho(z) \right)^{-1/2} \quad (7)$$

$$= \frac{3 \times 10^{12} M_\odot}{(1+z)^{3/2}} \left(\frac{\sigma_0}{300 \text{ km s}^{-1}} \right)^3 \left(\frac{f_*}{0.1} \right)^4, \quad (8)$$

which is so large that in practice all of our simulated galaxies would expel all their baryons if wind energy coupled efficiently with the remaining gas in the galaxies' halos. In Figure 7 we will show that this does not happen, and halos actually retain much of their baryonic mass far below the reheating scale. Hence in our models, the outflow energy does not couple efficiently to the ambient ISM or halo gas, but rather tends to blow holes and escape into the IGM. This idea is qualitatively consistent with high-resolution individual galaxy simulations of outflows (e.g. Mac Low & Ferrara 1999), but inconsistent with the assumption of efficient energy coupling with ambient gas that is sometimes made in analytical blowout models.

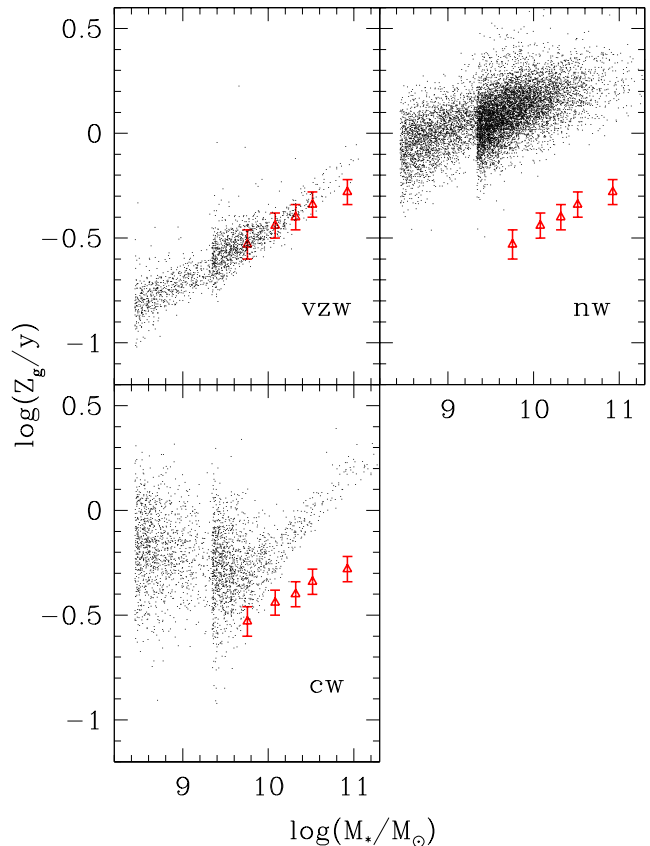


Figure 1. The MZR at $z = 2$ compared to observations by Erb et al. (2006) (reproduced from Davé et al. 2006b). The no-wind case overproduces metals, the constant wind case shows too steep a slope above the blowout scale and a large scatter below it, and the momentum-driven wind scenario fits observations quite well. The two clumps of points in each figure correspond to the 16 and $32h^{-1}$ Mpc simulation volumes, and are bounded at the low-mass end by their galaxy mass resolution limits.

3 THE $M_* - Z_G$ RELATION AT $Z = 2$

3.1 Gas-phase Metallicities

We begin by demonstrating that the choice of wind model heavily impacts the simulation's predictions for the MZR. Before doing so, several remarks are in order regarding the simulated and observed measurements. First, throughout this work we follow Davé et al. (2006b) and define the metallicity of each simulated galaxy as the SFR-weighted metallicity of its gas particles; this presumably provides a fair analogue to metallicities derived from metal emission lines as these trace the most actively star-forming regions in each galaxy. Second, in order to compare our simulated metallicities with the measurements of Erb et al. (2006) in Figures 1 and 11, we normalize all metallicities to the net yield. We have calculated the net Oxygen yield using published Type II SN yields (Woosley & Weaver 1995; Chieffi & Limongi 2004; Portinari et al. 1998) with the Salpeter (1955) and Chabrier (2003) IMFs and find that it lies between 0.008 and 0.021 depending on the choice of models, IMF, and metallicity. Our simulations assume a to-

tal metal yield of 0.02 with solar abundance ratios, corresponding to a net Oxygen yield of 0.0087. We use this value to normalize the Erb et al. (2006) measurements for consistency with our simulations while noting that the choice of net yield introduces a factor of ~ 2 uncertainty in the relative normalizations in Figure 1 that is in addition to the factor of ~ 2 uncertainty in the observed metallicities (Shapley et al. 2005). Finally, because the stellar masses reported in Erb et al. (2006) correspond to the total stellar mass formed whereas our simulations report the mass of stars that does not immediately explode in Type II supernovae, we multiply the Erb et al. (2006) masses by the ratio of mass in long-lived stars to the total mass formed (which is 0.802 for the Chabrier 2003 IMF) while noting that the observed stellar masses are also uncertain at the $\sim 2\times$ level owing to uncertainty in the IMF.

Figure 1 shows the MZR that arises in each wind model at $z = 2$, compared with observations by Erb et al. (2006). The fact that outflows affect the MZR is abundantly clear from these figures. In the no wind case, galaxies are too enriched at a given stellar mass (this is also seen in the wind-free models of De Rossi et al. 2006). This indicates that outflows are necessary to expel metals from galaxies, adding to the growing body of evidence that outflows have a significant and ubiquitous impact on high-redshift galaxies. Interestingly, the slope of the MZR in the no-wind case is in fair agreement with observations (though slightly too shallow in detail), despite the fact that no galaxies are driving out any metals. Metal loss by tidal stripping is generally negligible, as we show in §5.3. Hence the slope of the MZR does *not* necessarily imply that low-mass galaxies preferentially expel metals relative to high-mass ones. Even without outflows, the observed MZR slope (though not its amplitude) is broadly reproduced.

The constant wind (cw) model shows some remarkable and interesting trends. Above the blowout scale of $10^{10} M_{\odot}$, the MZR slope is quite steep, steeper than the no-wind case, and the scatter is fairly small. Hence relative to the no-wind case, the cw model appears to be preferentially ejecting metals from low-mass systems, as expected. Unfortunately, this takes what was a good agreement with the observed slope in the nw case and produces poor agreement in the cw case. Below the blowout scale, the scatter increases dramatically; this behavior is seen at all redshifts down from $z \approx 6 \rightarrow 0$ and is not a consequence of numerical resolution, as evidenced by the fact that our higher-resolution run joins smoothly onto the lower-resolution one. The large scatter in the cw model can be qualitatively compared with the findings of Geha et al. (2006), who report that the observed baryonic Tully-Fisher relation does not show the excess scatter below the blowout scale that would be predicted in blowout scenarios. Additionally, Lee et al. (2006) have shown that the observed scatter is ≈ 0.1 dex at all mass scales at low redshift and argued that this is inconsistent with blowout scenarios. We discuss the likely source of this excess scatter in Section 7.5; the important point is that this scatter is not observed, hence models that introduce a characteristic blowout scale at observable masses are unlikely to be consistent with Lee et al. (2006).

The vzw model’s MZR shows good agreement with observations in both slope and amplitude. There is a minor offset in amplitude, but there are enough systematic uncertain-

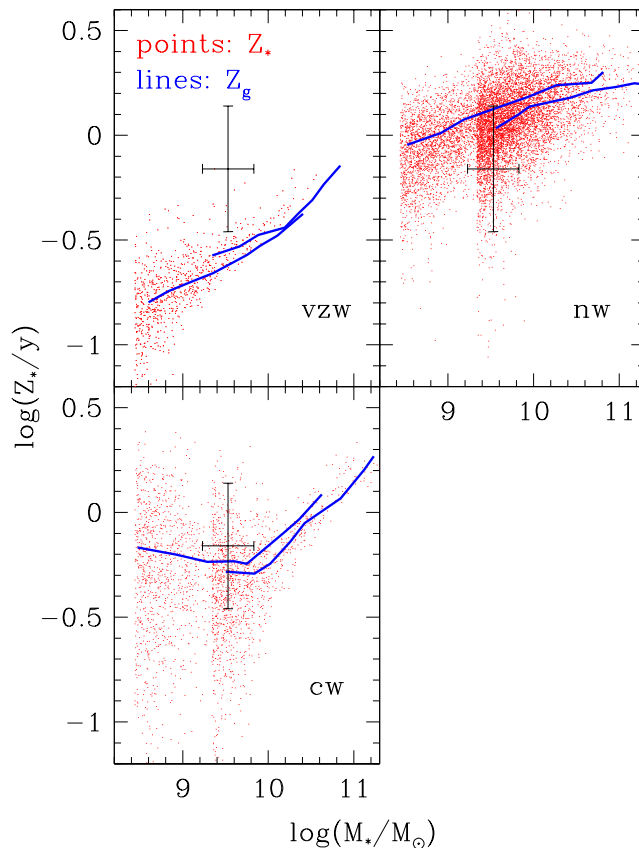


Figure 2. Z_* versus M_* at $z = 2$. Red dots denote galaxies in our simulations while blue curves denote the mean trend from the gas-phase MZR (Figure 1). The data point with error bars denotes the inferred stellar mass and metallicity of MS 1512-cB58. Within each wind model, the UV-weighted stellar metallicities closely track the metallicity of the star-forming gas, as expected.

ties in metallicity indicators to render this difference insignificant (e.g. Tremonti et al. 2004; Ellison & Kewley 2005). To explain this agreement, Davé et al. (2006b) proposed that galaxies must lose a roughly fixed fraction of their metals independent of their mass, because this would preserve the slope seen in the nw case while lowering the amplitude. Indeed, by comparing the mass of metals produced by each galaxy in the vzw run with the mass of metals retained in stars and gas, we find the fraction of metals that galaxies retain scales very slowly as $M_*^{0.07}$ at $z = 2$ (§5.3). It is intriguing to compare this result to Geha et al. (2006), who infer that the fraction of baryons lost cannot vary with baryonic mass based on the fact that the slope of the observed $z \sim 0$ baryonic Tully-Fisher relation lies very close to the value that is expected from cosmological simulations that do not treat baryons. In the momentum-driven wind scenario this arises naturally because outflow speeds scale with galaxy escape velocities.

3.2 Stellar Metallicities

Although the goal of this paper is to understand the relationship between stellar mass and gas-phase metallicity,

recent observational efforts to constrain the evolution of the stellar mass-stellar metallicity relation (hereafter, the “stellar MZR”) motivate a comparison between our simulated gas-phase and stellar metallicities. Before we proceed, however, a few comments on systematic effects are in order. The first observational constraints on the high-redshift stellar MZR will focus on rest-frame UV absorption features (e.g., the 1978 index of Rix et al. 2004) because at $z \geq 2$ these features are redshifted into conveniently-accessible optical wavelengths. Unfortunately, they are also dominated by stars with zero-age main-sequence masses greater than $5M_{\odot}$ (Rix et al. 2004), hence they are only sensitive to a galaxies’ youngest stars. In order to estimate the extent to which the observed stellar MZR depends on the choice of metallicity indicator, we have measured the stellar MZR for each wind model twice: once using mass-weighted stellar metallicities averaged over all stars ($Z_{*,\text{all}}$), and once using only stars that are younger than 100 Myr ($Z_{*,\text{UV}}$). The latter figure approximates a UV-luminosity-weighted stellar metallicity. We find that, for all three wind models, $Z_{*,\text{UV}}$ lies systematically 40–60% higher than $Z_{*,\text{all}}$, indicating that UV indices systematically overestimate stellar populations’ mean metallicities even in the absence of any systematics in the indices themselves. We also find that, in all three wind models, the scatter in $Z_{*,\text{UV}}$ at given M_* is 0.1–0.2 dex, whereas the scatter in $Z_{*,\text{all}}$ is generally ≈ 0.05 dex, tighter than the scatter in the gas-phase MZR. The increased scatter in $Z_{*,\text{UV}}$ likely owes partially to our simulations’ limited mass resolution. On the other hand, it is also likely that the short time baseline sampled by UV indices renders them more sensitive to the distribution of metallicities among individual HII regions within individual galaxies, hence we do expect the scatter in the measured MZR to be larger for UV indices than for optical indices. In order to facilitate comparison with upcoming measurements at high redshift, we only consider $Z_{*,\text{UV}}$ throughout the rest of this work.

The red points in Figure 2 compare the predicted stellar MZR at $z = 2$ for our three wind models (red points) to the mean gas-phase MZR (blue curves) as well as to current constraints on the $z = 2.7276$ lensed galaxy MS 1512-cB58 (hereafter, “cB58”; Yee et al. 1996). For cB58, we use the stellar metallicity of Rix et al. (2004) normalized to solar yield and the stellar mass of Baker et al. (2004). We assume a factor of 2 uncertainty for each estimate. Comparing the stellar and gas-phase MZR in Figure 2 indicates that they are predicted to be quite similar, regardless of the outflow scenario. This is expected since young stars’ metallicities should track the metallicities of their parent gas clouds. On the other hand, it is not consistent with observations of cB58, for which the most likely stellar metallicity $Z_* = 0.7Z_{\odot}$ significantly exceeds the inferred gas-phase metallicity $Z_g = 0.4 \pm 0.1Z_{\odot}$ (Rix et al. 2004). However, considering that the metallicity offset in cB58 is well within the range of systematic uncertainties and that its ISM metallicity shows excellent agreement with the observed mean gas-phase metallicity for its stellar mass at $z \sim 2$ (Erb et al. 2006), we believe that the offset likely results from systematic offsets in the observational abundance indicators. It will be interesting to see whether larger samples of galaxies at high redshift show a similar offset.

We have additionally compared our stellar MZR to the stellar MZR predicted at $z = 2$ by the hypernova feedback

model of Kobayashi et al. (2007, Figure 20). In the range $10^9 - 10^{10.5} M_{\odot}$, the Kobayashi et al. (2007) model predicts V-band luminosity-weighted stellar metallicities that are ≥ 0.5 dex below our nw model at all scales, 0.1–0.2 dex higher than our vzw model at all scales, and 0.2–0.5 dex below our cw model at all masses except the blowout scale. The best agreement is hence with our favored vzw model, indicating that, broadly, the effects of the Kobayashi et al. (2007) hypernova feedback model are similar to our momentum-driven outflows although the hypernova winds may be somewhat weaker.

3.3 The IGM Metallicity

A fully self-consistent model for galaxy evolution must account for the distribution of metals in the IGM as well as in galaxies, hence we have also tested our outflow models by comparing the predicted and observed IGM metallicities. Because the impact of our outflow prescriptions on the distribution of metals in different gas phases has been discussed previously (Oppenheimer & Davé 2006; Davé et al. 2007), we will only mention the results here. The mean metallicity of the IGM at $z = 2$ in our favored vzw model is roughly $[Z/H] = -1.7$ (Davé et al. 2007, Figure 1). This is roughly twice as high as predicted by the hypernova feedback model of Kobayashi et al. (2007, Figure 18), implying once again that the outflows in the hypernova feedback model are somewhat weaker. However, by analyzing simulated quasar absorption spectra generated along sightlines through the simulation volume, Oppenheimer & Davé (2006) have shown that the predicted abundance of CIV in the vzw model is in excellent agreement with observations from $z = 6 \rightarrow 2$. Hence our favored vzw model is broadly consistent with observations of the distribution of metals both within and outside of galaxies at $z = 2$.

4 ANALYTICAL MODEL FOR THE MZR

Figure 1 strongly suggests that the observed MZR can be used to constrain superwind models, but it gives little physical insight into how superwinds impact the trends and evolutionary behavior of the MZR. In order to probe this question more deeply, we construct a simple one-zone chemical enrichment model similar to many others in the literature (e.g., Tinsley 1980). The novel aspect is that we will use our simulations to calibrate the model inputs, so essentially by construction our analytical model will broadly reproduce the simulation results, as we show in §6.3. Owing to its simplicity, it provides an instructive tool to examine the relative importance of various physical effects in driving the MZR, which we will do in §7.

4.1 Equations of Evolution

At each timestep, the mass of metals in the ISM M_Z increases owing to inflows and star formation and decreases owing to outflows and metals being locked up in long-lived stars:

$$\begin{aligned} \dot{M}_Z &= Z_{\text{IGM}} \dot{M}_{\text{ACC}} + y \dot{M}_{\text{SFR}} - Z_g \dot{M}_{\text{SFR}} - Z_g \dot{M}_{\text{wind}} \\ &= \alpha_Z Z_g \dot{M}_{\text{ACC}} + y \dot{M}_{\text{SFR}} - Z_g \dot{M}_{\text{SFR}} (1 + \eta_W) \end{aligned} \quad (9)$$

Here, Z_{IGM} and Z_g denote the metallicities of the IGM and the ISM, respectively; \dot{M}_{ACC} and \dot{M}_{SFR} denote the gas accretion and star formation rates, respectively; y denotes the net Oxygen yield (Tinsley 1980), \dot{M}_{wind} denotes the rate at which gas enters the wind; and η_{W} denotes the ratio $\dot{M}_{\text{wind}}/\dot{M}_{\text{SFR}}$. Equation 9 makes the following assumptions:

- The rate at which new metals are injected into the ISM is given by $y\dot{M}_{\text{SFR}}$, where the yield y is a constant;
- The outflow rate is proportional to \dot{M}_{SFR} ;
- The metallicity of the outflowing gas is equal to the mean metallicity of the galaxy’s ISM;
- We assume instantaneous feedback (Tinsley 1980) so that the effects of Type Ia supernovae and delayed mass loss are neglected;
- The mean metallicity of inflowing gas is some fraction $\alpha_Z \geq 0$ of the metallicity in the galaxy’s ISM;
- We neglect the difference between the rate of formation of all stars and the rate of formation of low-mass stars, i.e. we assume that the bulk of stellar mass is in long-lived stars; and
- All metals resulting from star formation and gas accretion are assumed to be well-mixed within the galaxy’s ISM.

The first four assumptions mimic those made in our simulations whereas the latter three are made for convenience. Also, note that any effects resulting from the enhanced cooling rates of metal-enriched gas will be taken into account implicitly when we tune our star formation efficiencies to match the simulations in Section 5.2.

To obtain the metallicity evolution in this model we need the evolution of metal mass as a function of gas mass. This requires us to know all the parameters in equation 9 except the net yield y (we normalize our metallicities by y in all of our Figures). We will assume $\alpha_Z = 0$ for the nw and cw models and 50% for the vzw model (we will justify this assumption in § 7.3). For η_{W} in the vzw model, we infer σ from the time-dependent relation between baryonic mass and velocity dispersion that we measure directly from the vzw outputs and then plug this into $\eta_{\text{W}} = 300 \text{ km s}^{-1}/\sigma$. For the cw model, we set $\eta_{\text{W}} = (2, 0)$ for all galaxies with masses (below, above) the blowout scale.

Finally, we need \dot{M}_{ACC} and \dot{M}_{SFR} as a function of redshift and galaxy mass. In the following sections we describe how we calibrate relations for these quantities from our simulations.

4.2 Gas Accretion History

We infer the time-dependent rate at which galaxies accrete fresh gas from their environments directly from the vzw simulations. In detail, we trace each galaxy’s baryonic growth rate backwards in time by searching for its most massive progenitor in each simulation snapshot. The total baryonic accretion rate is then simply the baryonic growth rate plus losses due to outflows:

$$\dot{M}_{\text{ACC}} = \dot{M}_{\text{bar}} + \eta_{\text{W}}\dot{M}_{\text{SFR}}. \quad (10)$$

In practice this technique yields the accretion rate of gas and stars rather than just gas as it is difficult to determine from the outputs of our simulations whether new stellar mass results from star formation or mergers. However, baryonic mass growth is known to be dominated by gas accretion at

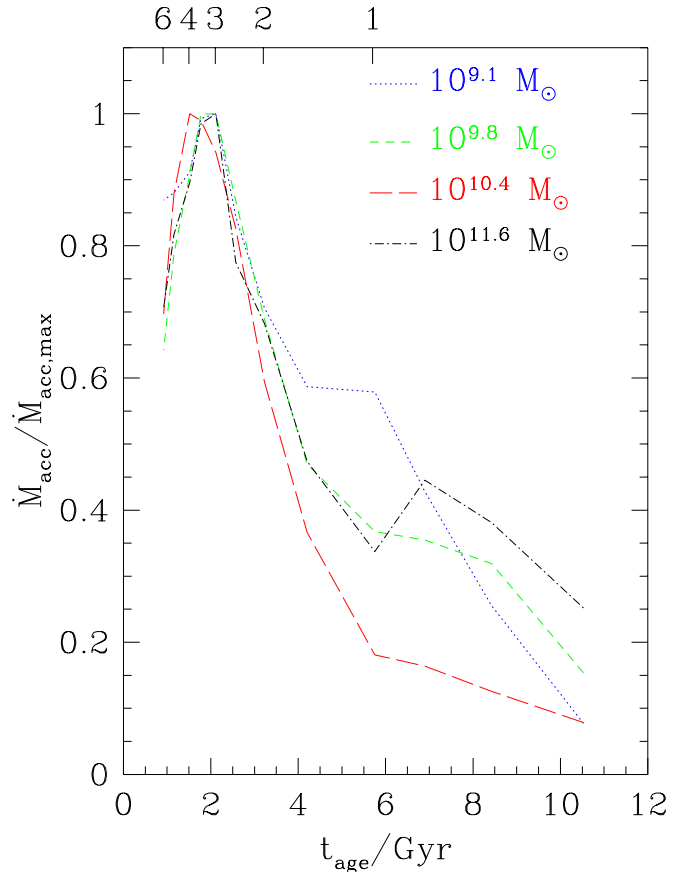


Figure 3. Mean baryonic accretion rates of the simulated galaxies in the $32h^{-1}\text{Mpc}$ vzw simulation as a function of time (bottom) and redshift (top). Four different mass bins are shown, with the labels referring to the stellar mass at $z = 0$; each history is normalized to its maximum accretion rate. Galaxies of all masses experience remarkably similar baryonic accretion histories.

high redshifts (Kereš et al. 2005; Guo & White 2007), and the bottom panel of Figure 14 suggests that this is approximately true in our models as well.

To estimate outflow losses for the vzw model, we need the average η_{W} for each galaxy as a function of time. We can obtain a good estimate by combining the known baryonic mass with the time-dependent relation between galaxy velocity dispersion and baryonic mass, measured directly from our simulations, and substituting this back into the relation assumed by our vzw model $\eta_{\text{W}} = (300 \text{ km s}^{-1}/\sigma)$. Figure 3 plots the resulting accretion histories in 4 bins of stellar mass, where we have normalized each one to its maximum accretion rate; the mean stellar masses in each bin at $z = 2$ are indicated.

Galaxies of all masses experience remarkably similar accretion histories in our simulations, with accretion rates rising steadily at early times until a peak around $z \sim 4\text{--}3$ and falling afterwards. The existence of this generic accretion history has two interesting implications. First, under the assumption that \dot{M}_{SFR} tracks \dot{M}_{ACC} (which we justify below), the rising accretion rates immediately explain why galaxies generically exhibit rising star formation histories at high redshifts in our simulations (Finlator et al. 2007). Second,

the existence of a generic accretion history implies that a correlation between \dot{M}_{SFR} and halo mass—and, under reasonable assumptions, stellar mass—is expected, as found in other simulations by Finlator et al. (2006) and recently observed at $z \sim 0.5 - 2$ (Noeske et al. 2007; E. Daddi, private communication).

In detail, there are slight differences after $z = 2$ with a suggestion that the most massive galaxies continue to accrete too much gas at late times. Future work incorporating a treatment for AGN feedback is expected to alleviate this problem. Additionally, note that the use of a completely generic gas accretion history along with the assumption that the gas processing rate exactly tracks the gas accretion rate does not reproduce the so-called “downsizing” of galaxy evolution, where the latter is defined as the tendency for more massive galaxies to exhibit lower specific star formation rates (Zheng et al. 2007; Iglesias-Paramo et al. 2007), unless the ratio of past-averaged to present wind suppression factors $(1 + \tilde{\eta}_{\text{MLF}})/(1 + \eta_{\text{W}})$ scales strongly with mass. It is more likely star formation is delayed in low-mass galaxies by an effect that our model does not account for (Noeske et al. 2007b).

We averaged over the normalized accretion histories in Figure 3 and found that a reasonable approximation to the resulting mean accretion history is given by the fitting formula from Springel & Hernquist (2003b):

$$\dot{M}_{\text{ACC}}(z) \propto \frac{b \exp[a(z - z_m)]}{b - a + a \exp[b(z - z_m)]}. \quad (11)$$

Using a least-squares algorithm we determine the best-fit parameters for the vzw model as $a = 1.06$, $b = 1.32$, and $z_m = 3.5$. Although this formula was originally designed to describe the global star formation history, as Kereš et al. (2005) has pointed out, this closely tracks the gas accretion history, so it is not surprising that a good fit is obtained for \dot{M}_{ACC} using this form.

Similar trends are seen in the cw and nw models at $z \geq 2$ (unfortunately only our vzw simulations were evolved to $z = 0$). In detail, there are slight differences between the gas accretion histories in the three wind models. The most prominent of these is that gas accretion rates peak at an earlier redshift in the cw model than in the vzw or nw models because the cw’s energetic winds heat the IGM too efficiently (Oppenheimer & Davé 2006). As a result, the gas cooling time at moderate overdensities (~ 10) surpasses a hubble time and the star formation rate density begins to decline at an earlier redshift ($z \sim 5$; Springel & Hernquist 2003b) than in the vzw or nw models ($z \sim 3$; Oppenheimer & Davé 2006). We account for this early peak by setting $z_m = 5$ when modeling the impact of cw outflows in our analytical model. We will show in Figure 12 that using this parameterized fit to the vzw model’s gas accretion history allows us to approximate the chemical evolution of our simulated galaxies in all three wind models, hence a more detailed discussion of the impact of outflows on gas accretion histories is beyond the scope of the present work. The amplitude of a galaxy’s gas accretion history is determined by a constant multiplicative factor.

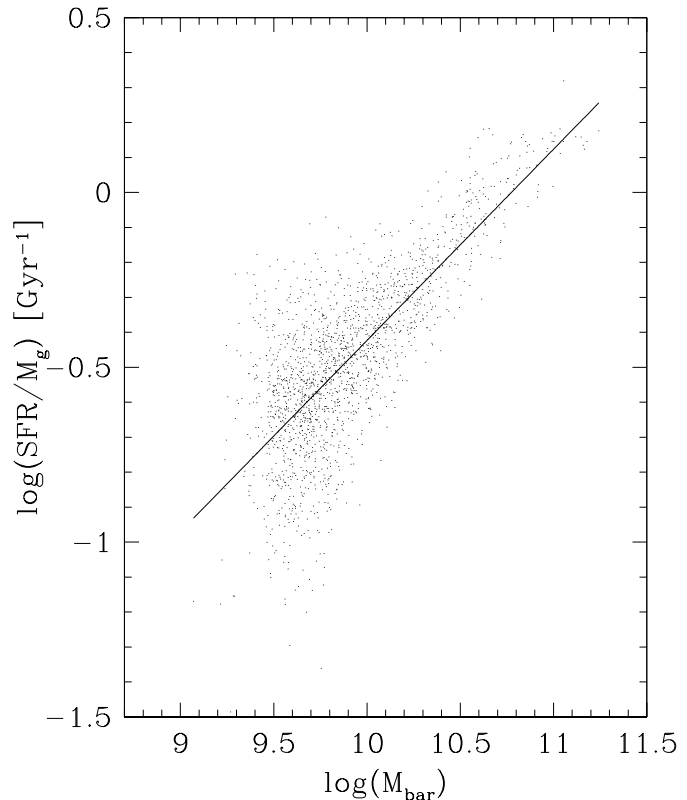


Figure 4. Least-squares fit to the vzw star formation efficiency at $z = 2$. Because the slope of the trend does not vary with scale, we can readily use it to tune our analytical model.

4.3 Star Formation Rates

To obtain \dot{M}_{SFR} , we measure \dot{M}_{SFR}/M_g in the simulations as a function of baryonic mass and redshift, and then use

$$\dot{M}_{\text{SFR}} = \frac{\dot{M}_{\text{SFR}}}{M_g}(z, M_{\text{bar}}) M_g, \quad (12)$$

where the gas mass M_g increases owing to inflows and decreases owing to outflows and star formation according to

$$\dot{M}_g = \dot{M}_{\text{ACC}} - \dot{M}_{\text{SFR}}(1 + \eta_{\text{W}}). \quad (13)$$

Through trial and error we determined that it is not possible to reproduce the detailed mass-metallicity evolution of our simulated galaxies without such a calibration for each wind model; indeed, this is a hint as to what governs the MZR.

Figure 4 shows that the star formation efficiency varies with scale in a simple way in the vzw model at $z = 2$; similar trends hold for all epochs and wind models. In order to tune our analytical model, we fit regression lines of the form $\log(\dot{M}_{\text{SFR}}/M_g) = a + b \log(M_{\text{bar}})$ to each simulation at a range of epochs. Figure 5 gives the resulting fits. In all three wind models $b > 0$, indicating that more massive galaxies are generically more efficient at converting their gas into stars owing to their higher gas densities; this behavior is qualitatively similar to the idea that star formation timescales are shorter in more massive galaxies (Noeske et al. 2007b). The offsets a in the wind models are everywhere lower than in the

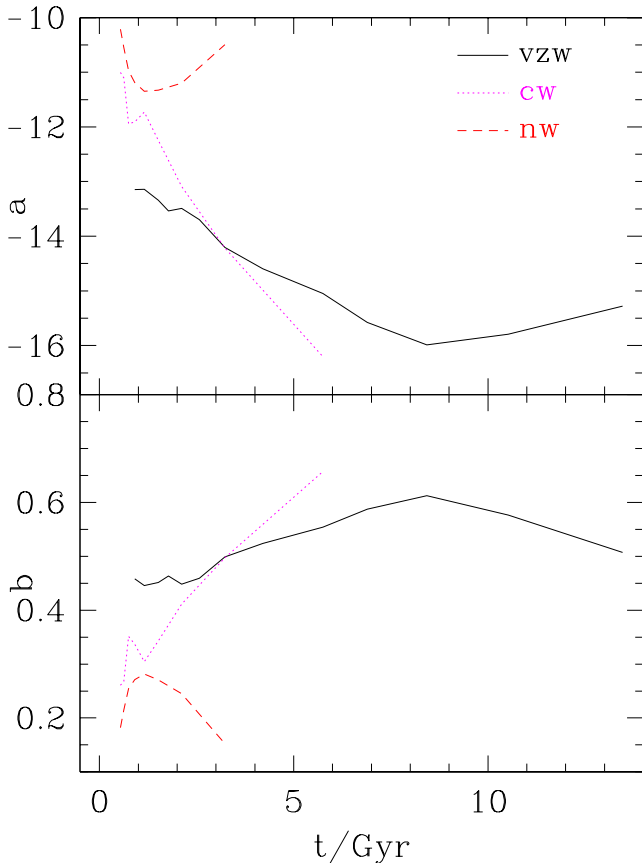


Figure 5. Least-squares fitting parameters to the star formation efficiency as a function of baryonic mass in our three wind models. For each model, the line indicates how fits to the relation $\log(M_{\text{SFR}}/M_g) = a + b \log(M_{\text{bar}})$ evolve over cosmic time.

nw model because superwinds decrease galaxies’ gas densities. The slopes b are everywhere higher in the wind models because wind effectiveness generically scales with mass. However, the fact that the cw efficiencies lie very close to the nw efficiencies at high redshift and then diverge from them suggests that cw winds are relatively ineffective in the low-mass galaxies that dominate at early times. The fact that the slope and offset of the trend evolve in opposite directions regardless of wind model indicates that gas densities in low-mass galaxies are more sensitive to changes in environment than in more massive galaxies. It is intriguing that the slope of the evolutionary trend changes sign near the point $z = 0.5$, likely a consequence of the universe becoming Λ -dominated.

Does self-enrichment impact our simulated star formation efficiencies? If gas in more massive halos cools more efficiently owing to enhanced metallicities then a scale-dependent “positive feedback” could obtain between the gas cooling and self-enrichment rates; in this case the form of the MZR could be influenced by the relative effectiveness of this positive feedback cycle as a function of mass. Comparing Figures 1 and 5 shows that, indeed, the nw model exhibits both the highest star formation efficiencies and the highest metallicities, in qualitative agreement with this picture. However, the low star formation efficiencies in our wind

models can also be explained by the tendency for gas particles to be ejected by winds before their densities (and hence star formation rates) grow comparable to the typical densities in the nw model. Moreover, while the metallicities in the nw model scale more steeply than the vzw model, the star formation efficiencies scale more steeply in the vzw model, in qualitative disagreement with the self-enrichment picture. Additionally, we note that galaxy growth at these redshift and mass scales is dominated by cold-mode gas accretion (Kereš et al. 2005), with the result that the gas cooling timescale is much shorter than the dynamical timescale irrespective of its metallicity. In Section 7 we will show that, in the outflow model that reproduces observations, the MZR can be understood entirely in terms of the effects of outflows. Hence while a self-enrichment feedback cycle must be operating on some level, its effects on the observable MZR are likely to be weak compared to the effects of outflows.

5 THE EFFECTS OF WINDS

In this section we begin our exploration of the impact of outflows on the MZR by evaluating how winds affect our simulated galaxies; in short, we wish to determine what outflows *do* to galaxies. In our analytical model we assume that the primary parameters through which winds modulate the observable MZR are the star formation efficiency, η_W , and the gas accretion history. We would like to compare how each of these parameters scales with mass in our three wind models. The gas accretion history has been explored elsewhere (e.g. Oppenheimer & Davé 2006; Davé et al. 2006a), and is reasonably well described by equation 11. Hence we first discuss the impact of outflows on η_W and star formation efficiency. Next, we show that the fraction of metals retained by galaxies does not drive the MZR even though it is affected by outflows. Afterwards we compare how outflows suppress stellar mass and gas-phase metallicity on a galaxy-by-galaxy basis. Finally, we discuss how winds impact the trajectories that galaxies follow through the MZR.

5.1 Mass Loading

In our simulations, the rate at which material enters the wind is given by $\dot{M}_{\text{SFR}}\eta_W$. In the cw model, $\eta_W = 2$ and $V_W = 484 \text{ km s}^{-1}$ while in the vzw model $\eta_W = 300 \text{ km s}^{-1}/\sigma$ and $V_W \approx 6.7\sigma$. After a wind particle leaves the star forming region it interacts with the galaxy’s halo hydrodynamically. Some gas particles may escape into the IGM while others may radiate away their kinetic energy and rain back down as “galactic fountains”. Hence it is not obvious what fraction of the gas that enters a galaxy’s wind will actually escape from the galaxy permanently, or whether this fraction will preserve the input η_W scaling. Fortunately, the connection between star formation, metal enrichment, and winds allows us to constrain this quantity.

If an isolated star-forming galaxy generates a wind with a constant mass loading factor η_W then the fraction of metals that it retains is given by

$$\frac{M_{Z,\text{retained}}}{M_{Z,\text{formed}}} = 1 - \frac{\eta_W}{1 + \eta_W} \left(1 - \frac{Z_g M_g}{y M_*} \right). \quad (14)$$

If the masses and metallicities of a galaxy’s gas and stellar

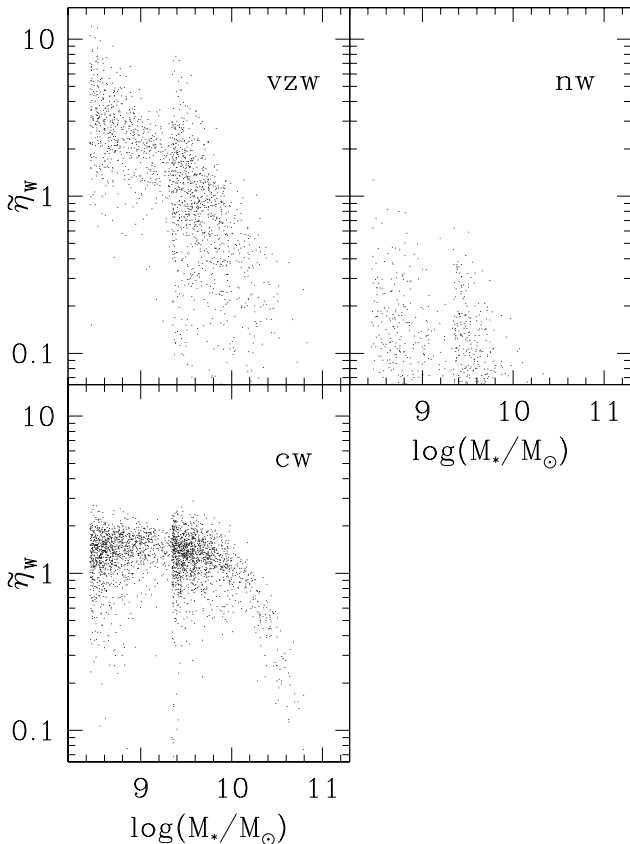


Figure 6. Mean mass loading factor experienced by galaxies as a function of stellar mass. In the nw model only low-mass galaxies lose any baryons, while in the cw and vzw models galaxies the mass of baryons lost scale as expected. Note how rapidly winds become ineffective above the blowout scale in the cw model.

phases are known then Equation 14 can be solved for the instantaneous mass-loading factor η_W . In general, η_W varies as the galaxy grows so that it is not possible to recover η_W from our simulation outputs. However, in this case it is still possible to obtain an “effective mass loading factor” $\tilde{\eta}_{\text{MLF}}$ as a function of stellar mass in our simulations from Equation 14 using the known masses and metallicities of the simulated galaxies; in this case $\tilde{\eta}_{\text{MLF}}$ measures the mass loss rate averaged over the galaxy’s star formation history.

As previously noted by Dalcanton (2006), the fact that equation 14 is not in general proportional to the effective yield indicates that the relative metal contribution to the IGM from different galaxies cannot straightforwardly be inferred from their effective yields (as attempted by, e.g. Bouché et al. 2007).

Figure 6 shows $\tilde{\eta}_{\text{MLF}}$ vs. M_* in our various wind models at $z = 2$. This plot is one of the most important ones in this paper for understanding the MZR. Looking at the nw model first, we find that $\approx 10\%$ of the nw galaxies show evidence of having lost some of their baryons ($\tilde{\eta}_{\text{MLF}} > 0$). These losses owe primarily to tidal stripping, although additional scatter is introduced by discreteness effects and uncertainties in the identification of low-mass galaxies within the simulation outputs. The result is a slight “flaring” of the trends toward

low masses that is visible in all three of our models. Because these effects are small compared to the overall trends that relate to the MZR (for example, compare the size of the $\tilde{\eta}_{\text{MLF}}$ in the nw model to the typical $\tilde{\eta}_{\text{MLF}}$ in the vzw model), they do not affect any of our results.

In the cw model, below the blowout scale $\tilde{\eta}_{\text{MLF}} \approx 1.5 \approx \frac{3}{4}\eta_W$, indicating that on average $\frac{3}{4}$ of wind particles from these galaxies leave permanently. Above the blowout scale ($\approx 10^{10}M_\odot$ at $z \sim 2 - 3$) $\tilde{\eta}_{\text{MLF}}$ declines rapidly because these winds thermalize their kinetic energy efficiently and return to the source galaxy as galactic fountains. Such a phenomenon, if real, would leave clear signatures in the observed baryonic Tully-Fisher relation or MZR at this scale. As we discuss in §7, the absence of such features in observations argues against the cw model.

In the vzw model, $\tilde{\eta}_{\text{MLF}} \propto M_*^{-0.25}$, shallower than the predicted slope of $-1/3$ if the stellar mass is a fixed fraction of the halo mass. To understand this, in Figure 7 we show the stellar fraction f_* as a function of M_{halo} , and indeed we see that for the vzw case $f_* \propto M_{\text{halo}}^{1/3}$. Taking this into account, we find that $\tilde{\eta}_{\text{MLF}} \propto M_{\text{halo}}^{-1/3} \propto 1/\sigma$ as expected. This indicates that outflow processes preserve the assumed scalings once the scaling of f_* is accounted for as long as the galaxy is above the blowout scale. Furthermore, it indicates that in the vzw model the fraction of wind particles that escape the galaxy is roughly constant for all galaxy masses, as required by observations of the low-redshift baryonic Tully-Fisher Relation (Geha et al. 2006).

It is interesting to note that the $\tilde{\eta}_{\text{MLF}}$ trend in our vzw scenario is qualitatively similar to the trend of wind strength versus mass in Figure 16 of Kobayashi et al. (2007). In our work, this trend results directly from the assumed scaling of the instantaneous η_W while in Kobayashi et al. (2007) it results from their treatment for pressure-driven outflows from supernova and hypernova feedback.

5.2 Star Formation Efficiency

We now discuss the impact of outflows on the star formation efficiency. We seek to answer two questions: (1) What impact do outflows have on the integrated star formation efficiency f_* (defined as the fraction of baryons in a halo converted to stars as a function of halo mass) at $z = 2$?; and (2) How do outflows suppress f_* ? The latter question is of interest because the expected scalings depend on whether outflows couple efficiently with the remaining gas in the galaxy’s ISM as well as its ambient IGM. If coupling is poor then, for galaxies above the blowout scale, the f_* scaling should reflect the intrinsic η_W scaling. Alternatively, if coupling is efficient then the f_* scaling should reflect the condition that the feedback energy is comparable to the binding energy of the baryons in the halo (e.g., Dekel & Silk 1986; Dekel & Woo 2003).

Figure 7 (similar to Figure 5 of Davé et al. 2006a) shows how f_* varies with stellar mass in the different wind models at $z = 2$. Examining the nw model first, we see that in the absence of winds f_* climbs steadily with mass below $M_{\text{halo}} = 10^{11}M_\odot$ and then decreases slowly with increasing mass above the characteristic minimum mass scale for halos to be dominated by hot gas rather than cold gas (e.g., Birnboim et al. 2007). This shape qualitatively mimics the behavior predicted by Dekel & Woo (2003). However, since

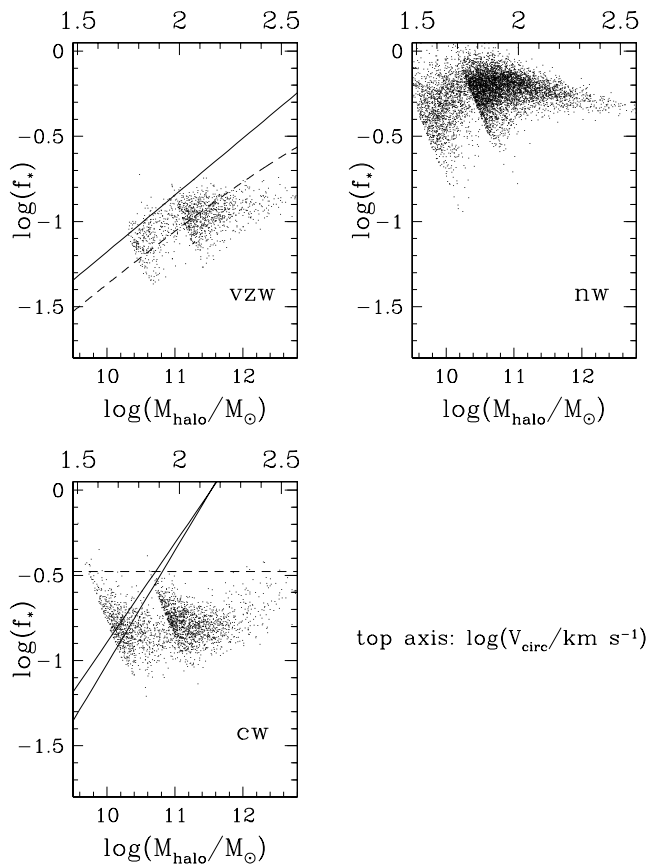


Figure 7. Fraction of baryons converted to stars as a function of halo mass (bottom axis) and circular velocity (top axis) at $z = 2$. The two loci correspond to halos from the 16 and $32h^{-1}\text{Mpc}$ volumes that contain more than 128 star particles. The dashed and solid lines in the wind models show the range of scalings expected from considerations of mass-loading and energy balance, respectively (Dekel & Woo 2003, see text). Below the minimum mass scale for hot-mode gas accretion f_* scales with mass even without outflows. In the presence of outflows, f_* is determined by the combined effects of mass-loading and Scannapieco & Broadhurst (2001) suppression.

there are no winds to couple the feedback energy to the halo gas, the qualitative agreement is merely a coincidence. The fact that f_* is not constant with stellar mass in the nw model has the important implication that f_* (and hence the MZR) is not governed solely by outflows (Dalcanton 2006). We note that Tassis et al. (2006, Figure 2) and De Rossi et al. (2006, Figure 2) have observed qualitatively similar behavior in the absence of strong outflows.

What determines the f_* scaling in the absence of outflows? If all halos converted their gas into stars with the same instantaneous star formation efficiency \dot{M}_{SFR}/M_g then neither Z_g nor f_* would scale with mass. Evidently \dot{M}_{SFR}/M_g must scale with mass at some point prior to $z = 2$. Indeed, we find that, without outflows, star formation efficiency and gas density increase strongly with increasing mass before the reionization epoch $z \geq 6$ although both trends weaken significantly by $z = 2$. The scaling in star formation efficiency at high redshift can be understood intuitively as a consequence of the fact that more massive

halos begin collapsing earlier than less massive halos, giving them a “head-start” in condensing their gas reservoirs. The same effect also manifests itself in a trend for more massive galaxies to exhibit older mean stellar ages than less massive galaxies in this model, dubbed “natural downsizing” by Neistein, van den Bosch, & Dekel (2006). As a result, low-mass galaxies possess lower gas densities, enhanced gas fractions and suppressed gas-phase metallicities with respect to massive galaxies.

The vzw model qualitatively resembles the nw model in f_* vs. M_{halo} except that it is shifted down by a factor of 5–12 with an additional dependence on mass (as shown more clearly in Figure 9). The normalization is lower because the vzw model significantly delays star formation (and suppresses gas-phase metallicities) at all scales. The flattening behavior in halos above $10^{11.5}M_{\odot}$ obtains because more massive halos are generally hot mode-dominated, just as in the nw model.

What determines the slope at masses below this scale? If we assume that, as the galaxy grows, the fraction of baryons that forms stars at each mass scale is $1/(1 + \eta_w)$, then f_* is simply given by

$$f_* = \frac{\int dM/(1 + \eta_w)}{\int dM}. \quad (15)$$

This scaling is denoted by the dashed line in the figure, where we have made the approximation that the halo velocity dispersion is given by $\sigma = 0.0083(M/M_{\odot})^{1/3} \text{ km s}^{-1}$. Alternatively, if we follow Dekel & Woo (2003) and assume that stars continue to form until the total energy in outflows equals the virial energy of the halo’s baryons then we find that $f_* \propto M^{1/3}(1+z)^{1/2}$ in the vzw model; this scaling is denoted by the solid line in the figure and has been normalized to 1 at the reheating scale at this redshift $M = 5.6 \times 10^{13}M_{\odot}$. At a glance the η_w -driven explanation seems more accurate although both theories produce the correct scaling. However, noting that the normalizations of these two scaling relations are somewhat uncertain owing to the assumptions in our spherical collapse estimates, in practice either explanation could be valid. Below we show that the f_* scaling that is expected from energy considerations is not obeyed in the cw model, implying that energy in outflows does not couple efficiently with inflowing material. For this reason we conclude that the accuracy of the f_* scaling that is predicted from energy considerations is purely a coincidence and that f_* is dominated by the scaling of the mass loading factor η_w .

In the cw model f_* is relatively flat between the smallest halos containing ≥ 128 star particles and the blowout scale at a halo mass of $10^{11.5}M_{\odot}$. Above the blowout scale f_* climbs slowly. The way that f_* varies only slowly with mass below the blowout scale and climbs above it echoes the cw model’s MZR (Figure 1), indicating a connection between the suppressed star formation efficiencies and the suppressed metallicities. However, the fact that Figures 1 and 7 look rather different in the cw model (especially above the blowout scale) indicates that the suppressed f_* does not by itself determine the MZR. Additionally, the fact that the MZR and the f_* plots look qualitatively different from the nw and vzw models indicates that some process specific to the cw model is affecting f_* and Z_g in similar ways.

What determines how f_* scales in the cw model? If f_* depended only on η_w then we would expect $f_* = 1/3$ at

all scales; this is indicated by the dashed line in the Figure. The slow dependence of f_* on M agrees qualitatively with the expected flat trend. However, the normalization is much lower than expected, indicating that another process must be suppressing galaxy growth. Returning to energy considerations, Dekel & Woo (2003) used the assumption that stars continue to form until the total energy in outflows equals the virial energy of the halo's baryons to predict that, in energy-driven wind scenarios such as our cw model, f_* (and hence the metallicity) should increase smoothly with increasing mass below the reheating scale of $\approx 150 \text{ km s}^{-1}$ and then flatten out above it. The range of possible scalings that they derive is indicated by the solid lines, where we have normalized their scalings to $f_* = 1$ at the reheating scale. Their predictions were based on the assumption that energy in outflows couples efficiently with the baryons in the galaxy's ISM and its halo. It is clear from Figure 7 that this key assumption does not hold in our cw model. At high masses the Dekel & Woo (2003) model predicts too little suppression, indicating that outflows suppress star formation even if much of the gas does not escape from the galaxy's halo. Furthermore, at low masses their model predicts too much suppression, indicating that simulated outflows either escape these galaxies without entraining the bulk of the halo gas (as would be expected if the outflows are not spherically symmetric) and/or their energy is thermalized and radiated away. Thus, despite the impressive agreement between observations and the simple model put forth by Dekel & Woo (2003), simulations suggest that the interaction between outflows and ambient gas is qualitatively different than what they assumed.

We can speculate as to why good agreement with the MZR is obtained by Dekel & Woo (2003), as well as in semi-analytic models based on this type of scenario such as De Lucia et al. (2004). In these models, they assume that winds from galaxies below the reheating scale inject progressively more energy per baryon into ambient gas, thereby unbinding progressively more of it to smaller masses. In essence, they force a scaling of $\tilde{\eta}_{\text{MLF}}$ with M_* that is similar to our vzw model (cf. Figure 6), by assuming that $\tilde{\eta}_{\text{MLF}} \gg \eta_{\text{W}}$ for small masses owing to efficient energy coupling with ambient gas. This physical process is not borne out by our three-dimensional numerical simulations, in which reheating is mostly irrelevant. It is a minor coincidence that in constant wind models, the blowout and reheating scales are fairly similar (equations 1 and 3).

In summary, a comparison between Figures 1 and 7 indicates that (1) in the presence of outflows, the scaling of f_* (or, equivalently, gas fraction) depends more heavily on the mass-loading factor η_{W} than on energetic considerations; and (2) f_* , while a key driver, does not by itself determine the MZR. Some other factor must be important in determining the basic shape of the MZR. We will argue below that it is primarily gas accretion, although gas stripping due to winds from neighboring galaxies can play a role in some situations, as we will discuss in In § 5.3 and 5.4.

5.3 Metal Retention

The most popular interpretation of the observed MZR is that low-mass galaxies exhibit low metallicity because they drive a larger fraction of their metals into the IGM. In order

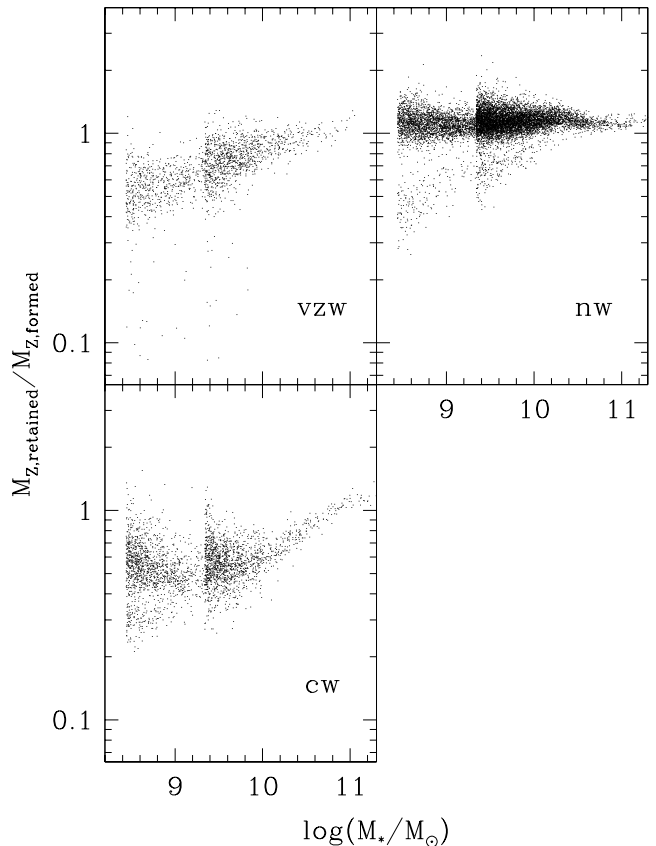


Figure 8. Fraction of metal mass retained $f_{\text{Z,ret}}$ as a function of M_* . The two loci correspond to galaxies from the 16 and $32h^{-1}\text{Mpc}$ volumes. Without winds galaxies tend to retain their metals, whereas in the presence of winds galaxies can lose up to 50% of their metals. These trends are far too weak to account for the observed MZR.

to determine whether this idea explains the observable MZR in our simulations, we plot in Figure 8 the fraction of metals retained $f_{\text{Z,ret}}$ as a function of stellar mass in each of our wind models. If metal loss dominates the form of the observable MZR then we expect the slope and scatter of $f_{\text{Z,ret}}$ as a function of M_* to mimic the MZR. For simplicity we discuss only the $16h^{-1}\text{Mpc}$ boxes at $z = 2$ here while noting that similar results hold for other scales and epochs.

In the nw model galaxies retain all of their metals on average (as expected in the absence of outflows) although ≈ 0.06 dex of scatter is introduced by dynamical disruption and uncertainties in group identification. This contrasts with the strong scaling ($Z_g \propto M_*^{0.28}$) and larger scatter (0.11 dex) in the nw MZR (Figure 1). Moreover, a few low-mass galaxies have lost up to 80% of their metals through interactions, yet we find that even these galaxies exhibit no departure from the mean gas-phase metallicities for their stellar masses. Hence while they have ejected significant baryons, those baryons were enriched at the same level as the baryons that remained in the galaxies.

Turning to the wind models, at a fiducial stellar mass of $10^{10} M_\odot$ the cw and vzw models retain roughly 40% and 70% of their metals at $z = 2$, respectively. However, the mean gas-phase metallicity of the cw galaxies is roughly 70%

higher than it is in the vzw galaxies. Comparing the scalings reveals similar inconsistencies: In the vzw model $f_{Z,\text{ret}} \propto M_*^{0.07}$ while the MZR scales as $Z_g \propto M_*^{0.21}$. In the cw model, $f_{Z,\text{ret}} \propto M_*^{-0.04}$ with 0.09 dex of scatter, while its MZR scales as $Z_g \propto M_*^{0.06}$ (note that this is in the opposite sense as the $f_{Z,\text{ret}}$ scaling) with 0.19 dex of scatter.

The poor correspondence between the $f_{Z,\text{ret}}$ scalings and the MZR for all three models indicates that galaxy metallicities are not primarily driven by metal loss. The inconsistency between the relative gas-phase metallicities and $f_{Z,\text{ret}}$ values of the vzw and cw models suggests that the detailed way in which metals are distributed in different baryonic phases must be taken into account. Note that we do not claim that $f_{Z,\text{ret}}$ cannot trace the MZR *in principle*; Figure 8 only shows that it does not do so in general. Indeed, there is no rigorous reason why it should. Observationally, it is possible to test this if the metallicities and masses in the stellar and gas phases as well as the net metal yield y are known: if $Z_g \propto f_{Z,\text{ret}}$ then it should also be proportional to $Z_*(y - M_g/M_*)^{-1}$ at all scales. However, guided by our own simulations, we will argue in §7 that the MZR is dominated by the scaling of the star formation efficiency in the absence of winds, and by a competition between the rates of enrichment and dilution in the presence of winds.

5.4 Suppression of M_* and Z_g

Another way to highlight the differences between the wind models is to compare their effects on individual galaxies. Because all of our simulations were run with the same initial conditions, we can readily do this by matching the positions of individual galaxies between the simulations. Figure 9 displays the ratios of stellar mass and metallicity in the wind models versus the no wind model at $z = 2$. Note that we have directly verified that excluding from Figure 9 those galaxies whose nw metallicities suggest $\tilde{\eta}_{\text{MLF}} > 0$ does not impact the slope, normalization, or scatter of the inferred suppression factors for either wind model.

In the cw model one might at first expect the ratios $M_{*,\text{cw}}/M_{*,\text{nw}}$ and $Z_{g,\text{cw}}/Z_{g,\text{nw}}$ to be $\approx 1/(1 + \eta_W)$ for galaxies below the blowout scale as long as outflows couple inefficiently with the ambient gas (i.e. if $\eta_W = 2$ then 2/3 of the baryons should be ejected in winds). Figure 6 showed that cw outflows are highly effective for all galaxies below the blowout scale, in that their effective mass loading factor is, on average, equal to 3/4 of the true assumed $\eta_W = 2$, hence we might expect $M_{*,\text{cw}}/M_{*,\text{nw}}$ to be roughly $1/(1 + 2.5) = 0.4$. Turning to Figure 9, we see that $M_{*,\text{cw}}/M_{*,\text{nw}}$ lies below this value even at the blowout scale, consistent with the existence of an extra source of suppression implied by Figure 7. Above the blowout scale the cw ratios climb with tight scatter, reaching unity at $M_* \approx 10^{11.3} M_\odot$.

Below the blowout scale $M_{*,\text{cw}}/M_{*,\text{nw}}$ varies slowly with decreasing mass and shows considerable scatter. At the lowest masses ($M_* < 10^9 M_\odot$) $M_{*,\text{cw}}/M_{*,\text{nw}}$ and $Z_{g,\text{cw}}/Z_{g,\text{nw}}$ actually climb with decreasing mass despite the fact that $\tilde{\eta}_{\text{MLF}}$ is constant in this range. We have verified that these trends continue to lower masses at higher mass resolution, hence the behavior is not an artifact of numerical resolution. Moreover, it clearly conflicts with the naïve picture above. In order to understand it, we must consider how winds might

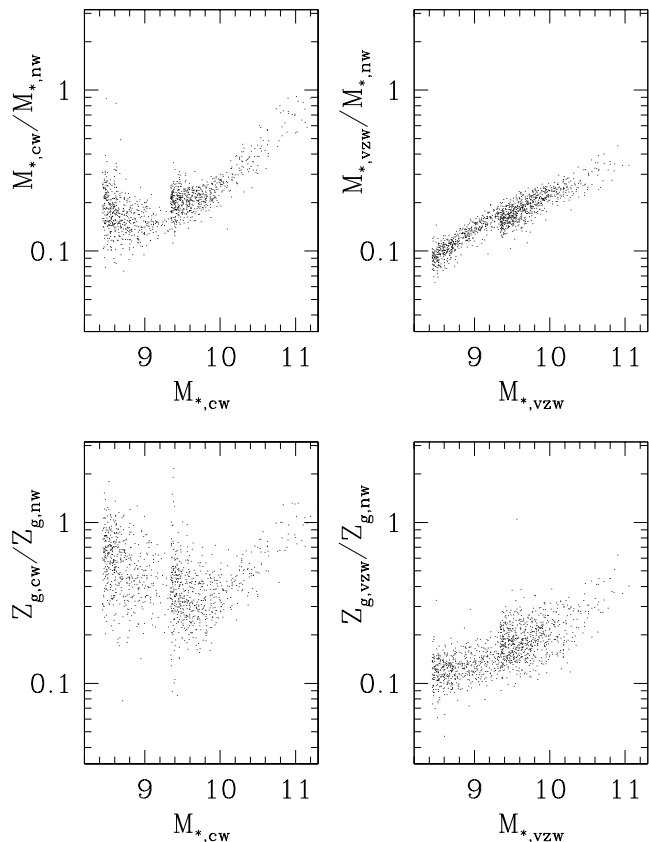


Figure 9. Ratio of stellar mass and gas-phase metallicity in the wind models versus the no-wind model at $z = 2$. The two loci correspond to galaxies from the 16 and $32h^{-1}\text{Mpc}$ volumes. In the cw model the effect of wind suppression does not vary strongly below the blowout scale whereas it decreases rapidly above it; in the vzw model wind suppression is less effective at higher masses and the scaling is quite smooth.

affect galaxy growth in the full context of structure formation rather than as isolated systems.

First, there is the possibility that an early generation of galaxies pre-enriches the IGM, giving rise to a “metallicity floor” in the observable MZR. Such a minimum has been inferred from quasar absorption line systems (e.g., Songaila 2001) as well as in our simulations (e.g. Davé et al. 2007). In Davé et al. (2006b) we hypothesized that widespread pre-enrichment of the IGM in the cw model (Oppenheimer & Davé 2006) may be responsible for its low-mass behavior. One way to quantify pre-enrichment is to measure how many metals were created in one galaxy, expelled, and reaccreted onto another. We measured the fraction of galaxies’ metals at $z = 2$ that originated in another galaxy and find that it is roughly 5% and 15% in the cw and vzw models, respectively. While this is not insignificant, it is not sufficient to account for the scatter in the cw MZR. Furthermore, the fact that the vzw model has more pre-enrichment but shows much less scatter suggests that this process does not contribute significantly to the MZR scatter. Hence the pre-enrichment hypothesis is unlikely to be correct.

Second, in a full hierarchical context there are two effects that reduce the tendency of winds to drain galaxies' gas reservoirs, which may lead to increased metallicities. Whereas in a simple closed-box scenario all gas is equally eligible to form stars, in a fully self-consistent model galaxies' gas reservoirs possess density and pressure gradients and star formation is concentrated in relatively small regions. Gas that is ejected from these areas can in principle be replaced on a dynamical time by infall from less dense areas owing to the loss of pressure support. A second effect is that gas entering a wind can potentially thermalize its energy before escaping the galaxy's halo and fall back down onto the galaxy in a galactic fountain, effectively increasing the galaxy's gas accretion rate. Figure 6 does not indicate the presence of scale-dependent galactic fountains below the blowout scale. On the other hand, the fact that $M_{*,\text{cw}}/M_{*,\text{nw}}$ increases at low masses suggests that gas that escapes the galaxy in a wind is indeed being rapidly replaced, boosting $M_{*,\text{cw}}/M_{*,\text{nw}}$ above what would naïvely be expected.

Finally, galactic winds can affect neighboring galaxies. In particular, Scannapieco & Broadhurst (2001) proposed that halos with masses $10^{9-10}M_{\odot}$ suffer stripping of their baryons owing to winds from lower-mass neighbors. In their model, once galaxies form they drive spherical winds whose energies are comparable to the wind energies in our cw model. The winds from galaxies in low-mass halos ($< 10^9M_{\odot}$) then strip baryons from intermediate-mass halos ($10^{9-10}M_{\odot}$) that are not yet virialized without affecting more tightly-bound massive halos ($> 10^{10}M_{\odot}$), with the result that galaxy formation in intermediate-mass halos is suppressed (note that this effect is not related to tidal stripping). Although our winds are not spherical, when averaging over a large sample of galaxies the effect should still be noticeable. It is expected to be weak at $z \geq 6$ (e.g., Figure 7 of Davé et al. 2006a) and to grow most noticeable during the heyday of galaxy formation $z \leq 3$ (Figure 8 of Scannapieco & Broadhurst 2001). Indeed, the ratios $M_{*,\text{cw}}/M_{*,\text{nw}}$ and $Z_{g,\text{cw}}/Z_{g,\text{nw}}$ show significantly less suppression at $z = 6$ (not shown) than at $z = 2$. More interestingly, they also show less scatter at higher redshifts, as expected for an effect whose strength depends on environment rather than on galaxies' intrinsic properties. In summary, it is likely that stellar mass growth in the cw model divides into three mass regimes: At low masses ($M_*/M_{\odot} < 10^8$) galaxy growth is suppressed only by outflows and hence $M_{*,\text{cw}}/M_{*,\text{nw}} \rightarrow 1/(1+\eta_{\text{W}})$. At intermediate masses ($10^8 < M_*/M_{\odot} < 10^{10}$) galaxy growth is dominated by a collaboration between Scannapieco & Broadhurst (2001) suppression and losses to winds, where the relative contribution of each effect varies nontrivially with scale and epoch. Because it only works in a particular mass regime, Scannapieco & Broadhurst (2001) suppression hence gives rise to a local minimum in $M_{*,\text{cw}}/M_{*,\text{nw}}$. Finally, at high masses ($M_*/M_{\odot} > 10^{10}$) galaxy growth is again dominated by outflows, where the effects of outflows weaken rapidly with increasing mass owing to the rapidly declining $\tilde{\eta}_{\text{MLF}}$ (Figure 6).

In the vzw model wind suppression of metallicity and stellar mass both scale smoothly, with relatively little scatter, and without evidence for a preferred scale. We have already shown (Section 5.2) that stellar masses in the vzw model can be attributed largely to the scaling of η_{W} . Given

that $f_{Z,\text{ret}}$ does not scale strongly with mass in this model, it is also not surprising that $Z_{g,\text{vzw}}/Z_{g,\text{nw}}$ scales in the same way.

Does baryonic stripping occur in our vzw simulation? We can predict whether it should be stronger or weaker in the vzw versus the cw model by estimating the ratio of their momentum generation rates:

$$\frac{\dot{p}_{\text{vzw}}}{\dot{p}_{\text{cw}}} = \frac{f_{*,\text{vzw}}\eta_{\text{W},\text{vzw}}V_{\text{W},\text{vzw}}}{f_{*,\text{cw}}\eta_{\text{W},\text{cw}}V_{\text{W},\text{cw}}} \quad (16)$$

From Figure 7, $f_{*,\text{vzw}} \approx 0.1$ and $f_{*,\text{cw}} \approx 0.2$. From before, we know $\eta_{\text{W},\text{vzw}} = 300 \text{ km s}^{-1}/\sigma$, $V_{\text{W},\text{vzw}} = 6.7\sigma$, $\eta_{\text{W},\text{cw}} = 2$, and $V_{\text{W},\text{cw}} = 484 \text{ km s}^{-1}$, hence we find that $\dot{P}_{\text{vzw}}/\dot{P}_{\text{cw}} \approx 1$ —the effect should be roughly as strong in the vzw model as in the cw model. By subtracting the mean trend from the vzw MZR and inspecting the residual, we have found that vzw galaxies less massive than $M_* = 10^{10}M_{\odot}$ do, in fact, exhibit signatures of baryon stripping, seen as a change of slope and a slightly increased scatter in the MZR below this scale. However, the effect is much less noticeable than in the cw model because it is small compared to the effects of the strong outflows. Applying this idea to interpret observations, the tight scatter and smooth scaling in the observed low-redshift MZR (Lee et al. 2006; Tremonti et al. 2004) indicate that either galactic winds do not carry enough momentum to suppress growth in neighboring halos appreciably or the effects of outflows must be strong enough to erase any evidence of baryon stripping; both possibilities clearly conflict with the behavior of our cw model, but are satisfied in our vzw case.

Comparing the top and bottom panels of Figure 9 yields insight into the extent to which f_* governs the MZR. The metallicity suppressions show considerably more scatter than the mass suppressions. Additionally, the gas-phase metallicities are systematically about 50% less suppressed than stellar masses in the cw models, independent of M_* . (They are roughly equally suppressed in the vzw model.) Both of these observations are inconsistent with the idea that f_* solely governs the MZR; evidently the effects of winds on gas accretion rates and star formation efficiencies also play a role.

In summary, Figure 9 indicates that outflows tend to suppress both M_* and Z_g . The trends and the levels of scatter indicate that the amounts of suppression cannot, in general, be predicted from simple scaling relations. We have highlighted the fact that, in both figures, the scatter in the cw model seems to be large below the blowout scale and small above it, whereas the scatter in the vzw model is comparable to ~ 0.1 dex at all masses. Lee et al. (2006) recently reported that the 1σ scatter in the observed relation is roughly 0.1 dex from 10^6 – $10^{12}M_{\odot}$ at low redshift and argued that this implied a less energetic form of metal-enhanced mass loss than blowouts. Our results tend to support this view. However, we also find that, in order to avoid the large scatter introduced by Scannapieco & Broadhurst (2001) suppression, winds must either transport significantly less momentum out of halos than occurs in the simplest energy-driven wind models, or else they must invoke large mass loading factors $\eta_{\text{W}} > 2$ at intermediate masses. Momentum-driven winds naturally satisfies that requirement while our constant wind model does not.

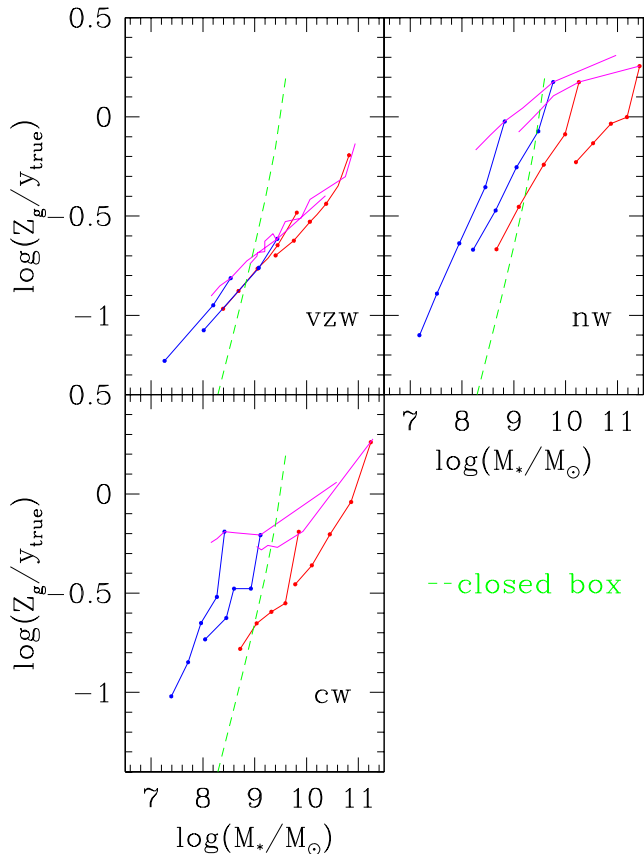


Figure 10. Mean enrichment histories of the simulated galaxies in the three wind models starting from $z = 6 \rightarrow 2$. Blue and red solid lines denote evolutionary trends from the 16- and $32h^{-1}$ Mpc boxes, respectively, while the green dashed line gives the slope of a closed-box with baryonic mass $5 \times 10^9 M_\odot$ ($Z_g/y = -\ln \mu(M_*)$). The magenta curves indicate the mean observable trends at $z = 2$. Galaxies evolve roughly parallel to the observable trend in the vzw model and more steeply in the cw and nw models.

6 EVOLUTION OF THE MZR

In the previous sections we explored how the effects of winds scale with mass by studying galaxies at a single epoch. In order to understand how outflows affect the *evolution* of the MZR, we now discuss how the metallicity evolves through cosmic time in our three models, as a function of galaxy mass and gas fraction. To do so, we trace the evolution of each simulated galaxy at $z = 2$ by searching for its most massive progenitor in each simulation output, thereby compiling its mass and metallicity history. Because enrichment histories of individual galaxies are highly stochastic, we bin the histories by stellar mass in order to show the typical evolution as a function of stellar mass.

6.1 Evolution of $M_* - Z_g$

Figure 10 compares the mean enrichment histories from the different models from $z = 6 \rightarrow 2$. As expected, galaxies generally increase in both mass and metallicity as they evolve. However, the slope of the evolution is in general neither constant nor parallel to the observable trend owing to the fact

that gas accretion rates, star formation efficiencies, and wind properties vary with scale and time. In particular, galaxies do not generally evolve as closed boxes (green dashed line) although the nw model comes quite close even at high redshift. Instead, their evolution is more shallow owing to the fact that outflows expel gas that is enriched compared to inflows from the IGM. At lower redshifts where strong outflows are rare and accretion rates are low, the evolution is expected to more closely resemble the closed-box scenario. This can be seen in Figure 1 of Brooks et al. (2006), where their simulated galaxies evolve from $z = 2 \rightarrow 0$ with a slope $d \log(Z_g)/d \log(M_*) \approx 1$. Additionally, Savaglio et al. (2005) have shown that closed-box scenarios can account for the observed evolution from $z = 0.7 \rightarrow 0.1$.

There is a slight upturn in the evolutionary slope from $z = 3 \rightarrow 2$ that can be seen in all three models. This feature occurs because gas accretion rates are declining during this interval owing to the increasing gas cooling times at intermediate overdensities; in other words, because gas accretion grows decreasingly effective at diluting gas reservoirs, star formation grows increasingly effective at enriching them. The fact that the rate at which the normalization of the MZR changes during this interval varies among our wind models illustrates how the time evolution of the MZR, in addition to its normalization, shape, and scatter, is a testable prediction of the wind model.

Turning to the individual models, galaxies in the nw model evolve nearly as steeply as a closed box in all but the highest mass bin. The relatively steep evolution in the low-mass bins reflects the fact that these galaxies' metallicities are not significantly diluted by inflows owing to their large gas fractions. By contrast, the shallower evolution in the highest mass bin indicates that, owing to their high gas densities and star formation efficiencies, these galaxies possess somewhat lower gas fractions with the result that inflows dilute their metallicities more readily. We will show in Figure 11 that the same effects can be seen in these galaxies' effective yields.

In the vzw model galaxies enrich their gas reservoirs somewhat more slowly. This evolution can intuitively be understood as a consequence of the tendency for vzw galaxies to expel a large fraction of their metals. However, we can also understand it via our analytical model as follows: In the vzw model, the effective mass loading factor scales with stellar mass as $\tilde{\eta}_{\text{MLF}} \propto M_*^{-0.25}$ (Figure 6). If galaxies' metallicities remain near equilibrium (Section 7.1) and if the gas processing rate is approximately equal to the gas accretion rate $\dot{M}_{\text{SFR}}(1 + \eta_w) \approx \dot{M}_{\text{ACC}}$, then the vzw MZR should scale with mass as $Z_g \approx y/(1 + \eta_w)$. For $\eta_w \gg 1$ (typical of small galaxies at high- z) we therefore expect $Z_g \propto M_*^{0.25}$ —exactly the scaling seen in Figure 10.

The evolution of the MZR in the cw model is more complex than in the other two models owing to the nontrivial environment-dependent interactions between the outflowing winds and the inflowing gas. The relevant points are that the basic shape of the constant wind MZR does not evolve with redshift while its normalization increases somewhat more rapidly than that of the vzw but not as rapidly as the nw model.

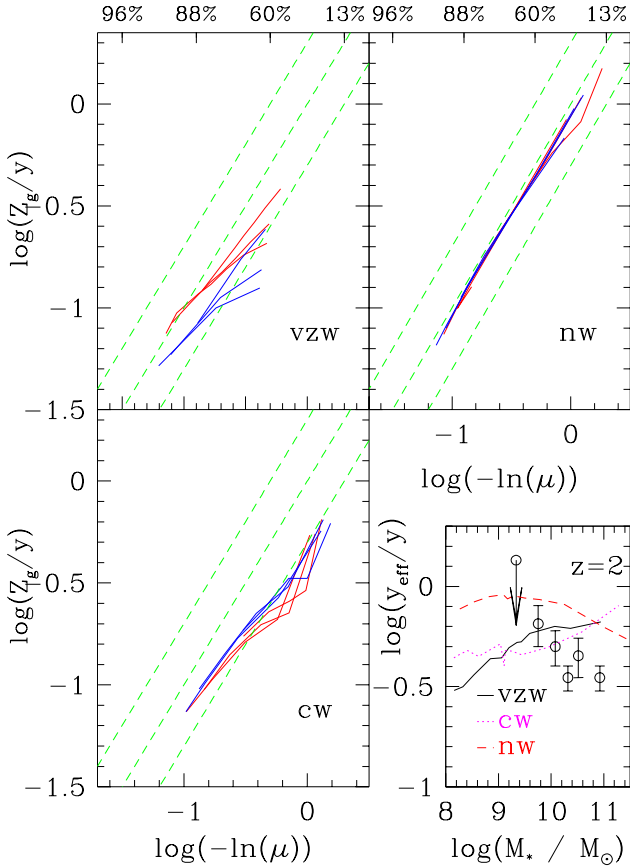


Figure 11. Mean enrichment histories of the simulated galaxies in the three wind models starting from $z = 6 \rightarrow 2$. Dashed green lines show where galaxies fall that have $y_{\text{eff}}/y = 0.5, 1.0, 2.0$. Blue and red solid lines denote evolutionary trends from the 16- and $32h^{-1}\text{Mpc}$ boxes, respectively. The nw galaxies involve much like closed boxes while the vzw and cw galaxies show suppressed effective yields.

6.2 Evolution of Effective Yields

A more direct way to investigate the extent to which our simulated galaxies depart from closed-box evolution is to plot the metallicity versus gas fraction, Figure 11. The axes in this figure are chosen so that galaxies with a constant effective yield $y_{\text{eff}} \equiv Z_g / -\ln(\mu)$ (where μ denotes the mass fraction of baryons in the gas phase) evolve along straight lines. The dashed green lines show the evolution for (from bottom to top) $y_{\text{eff}}/y = 0.5, 1.0, 2.0$. Individual galaxies generally evolve from lower left to upper right in this space.

The nw galaxies remain quite close to the closed-box curve $y_{\text{eff}}/y = 1.0$ as suggested by the steep evolution in Figure 10. The effective yield never exceeds the closed-box case, as required by Theorem 3 of Edmunds (1990). It drops below the closed-box value most strongly at the redshift corresponding to the peak accretion rates $z \approx 3$ because the dilution of the metallicities at this epoch is overcompensating for the increase in gas fraction (this happens irrespective of the wind model and is therefore a robustly predicted—if difficult to confirm—consequence of the global gas accretion peak at $z \approx 3$). After the accretion rates begin subsiding,

y_{eff}/y returns to the closed-box value relatively quickly owing to continued star formation (Dalcanton 2006).

By contrast, galaxies in the vzw model tend to evolve from higher to lower y_{eff}/y during this period owing to the combined effects of dilution and outflows. In this model accretion rates fall off somewhat more slowly following the $z = 3$ peak than in the other models, pushing the peak of star formation to lower redshift (Oppenheimer & Davé 2006) and delaying the recovery of the effective yields. The delayed falloff in accretion owes to galactic fountain effects that occur because outflowing gas does not escape the halo $\sim 20 - 50\%$ of the time, on average. The gas is then retained in a puffy distribution, owing to small wind speeds that do not drive gas far from the galaxy, and becomes available for reaccretion on a time scale smaller than a Hubble time.

Galaxies in the cw model show a gradual evolution from nearly closed-box yields $y_{\text{eff}}/y \approx 0.8$ at $z = 6$ to lower values $y_{\text{eff}}/y \approx 0.3$ at $z = 3$ before rebounding to $y_{\text{eff}}/y \approx 0.5$ at $z = 2$. The relatively weak dependence of y_{eff}/y on M_* at all redshifts recalls the flat MZR in Figure 1 and owes to the fact that most of the galaxies in this figure lie below the blowout scale and are hence roughly equally affected by winds.

The bottom-right plot in Figure 11 compares how y_{eff} varies with M_* at $z = 2$ in our three models versus observations of UV-selected galaxies at $z \sim 2$ (Erb et al. 2006). The nw model shows no trend at low masses and declines with increasing mass for masses above $10^{10}M_\odot$. The decline occurs because gas fractions decline with increasing mass: Galaxies more massive than $10^{10}M_\odot$ have gas fractions $\mu \leq 20\%$ in the nw model so that unenriched inflows are able reduce y_{eff} efficiently (Dalcanton 2006). The y_{eff} behavior is qualitatively consistent with the observed trend although the normalization is $\approx 50\%$ too high.

In the vzw model, y_{eff} increases with increasing mass at low masses and flattens out around $10^{10}M_\odot$. This behavior at face value conflicts with observations at $z \sim 2$. On the other hand, it bears a striking resemblance to the observed trend at low redshift (Garnett 2002; Tremonti et al. 2004; Pilyugin et al. 2004). Although we do not show it here, the overall shape of the y_{eff} trend in the vzw model does not vary with redshift. An aggressive interpretation of Figure 11 would be that winds at high redshifts must differ qualitatively from winds at low redshifts, with the former relatively more effective in massive galaxies than the latter; in other words, at high redshift the effect of winds on y_{eff} should preserve the nw scaling while at low redshift the vzw model is more realistic. However, considering that Erb et al. (2006) were forced to infer gas masses indirectly rather than measuring them, and given that their measurements span a much smaller dynamic range than low-redshift observations, we prefer not to draw any firm conclusions from Figure 11. Future measurements that trace high-redshift gas masses more directly (e.g. with ALMA) will constrain the effective yields of high-redshift galaxies more directly, and will provide a key test of the momentum-driven wind scalings.

The vzw trend at low masses is expected despite their higher gas fractions (not shown) because η_W increases to lower masses (Figure 6). In terms of our analytical model, we now anticipate the conclusions of Section 7 by assuming that $\dot{M}_{\text{SFR}}(1 + \eta_W) = \dot{M}_{\text{ACC}}$ and dividing Equation 20 by

$y \ln(1/\mu)$ to find the equilibrium condition:

$$\frac{y_{\text{eff,eq}}}{y} = \frac{1}{(1 + \eta_W) \ln(\frac{1}{\mu})} \quad (17)$$

As mass increases, η_W decreases (Figure 6), hence $y_{\text{eff,eq}}$ increases.

The flattening behavior in $y_{\text{eff,eq}}$ around $M_* = 10^{9.5-10} M_\odot$ is more interesting. Recall that in our vzw model the fraction of baryons lost to winds does not vary strongly with mass (Section 5.3). Evidently, a flattening in y_{eff} does not necessarily indicate a scale at which superwind feedback becomes effective at removing a galaxy’s metals, an interpretation we discuss further below. Nor does it indicate that y_{eff} has reached the true yield $y_{\text{eff}}/y = 1$. Instead, it seems to be a coincidence resulting from a competition between dilution owing to accretion and the outflows’ suppression of star formation. Indeed, in more massive galaxies ($M_* > 10^{11} M_\odot$) y_{eff} begins to increase with mass again owing presumably to the fact that gas accretion rates are falling in this range. While the highest mass bin in the Tremonti et al. (2004) data tantalizingly suggests agreement with this behavior, confirmation will have to await the arrival of larger samples of massive star-forming galaxies at $z \sim 1$ (since at $z = 0$ massive galaxies are generally too gas-poor for their gas-phase abundances to be measured).

Garnett (2002) also found a flattening of y_{eff} below $\sim 100 \text{ km s}^{-1}$ at low redshift, but his interpretation was that low-mass galaxies retain a smaller fraction of their metals owing to the onset of winds in less massive galaxies, in conflict with our interpretation. However, Dalcanton (2006) recently used the same data to show that the observed trend in y_{eff} can be obtained without assuming that winds are more effective in low-mass galaxies by removing the approximation that the gas fraction is constant. In this view, y_{eff} is suppressed in low-mass galaxies because their low star-formation efficiencies prevent their y_{eff} from recovering quickly from inflow episodes. Our findings tend to support the latter view.

In the cw model, y_{eff} does not vary with mass below the blowout scale and increases with increasing mass above it, emphasizing the idea that the effectiveness of winds below the blowout scale does not seem to follow the trends that would be expected from simple scaling arguments.

Effective yields can also give insight into another important question in the study of high-redshift galaxies, namely whether the buildup of stellar mass occurs in a predominantly smooth or episodic fashion. At redshifts $z < 1$, the tight observed correlation between stellar mass and \dot{M}_{SFR} argues in favor of a predominantly smooth mechanism for relatively massive galaxies $10^{10} < M_*/M_\odot < 10^{11}$ (Noeske et al. 2007). At $z \sim 2$, clustering measurements indicate that Lyman-break and submillimeter galaxies possess duty cycles of ~ 1 (Adelberger et al. 2005a) and ~ 0.1 (Bouché et al. 2005), respectively, suggesting that Lyman Break galaxies form stars smoothly while submillimeter galaxies are more bursty. Similarly, recent clustering measurements indicate that Lyman- α emitters at $z \approx 4.5$ possess duty cycles of $\sim 10\%$, again hinting at relatively bursty star formation histories (Kovac et al. 2007).

Effective yields provide another way to test this behavior, because in the absence of inflows and outflows, galaxies’ effective yields quickly recover to the true yield. Hence if the

timescale for the y_{eff}/y to recover to the true yield is short compared to the duty cycle then some mechanism must be actively suppressing it (Dalcanton 2006). Quantitatively, if we define the ratio of the effective yield to the true yield $X_y \equiv y_{\text{eff}}/y$ then, in the absence of inflows and outflows, X_y varies with time according to

$$\frac{d X_y}{d t} = \frac{\dot{M}_{\text{SFR}}}{M_g \ln(\frac{1}{\mu})} (1 - X_y) \quad (18)$$

This equation shows that the equilibrium solution $X_y = 1$ is a stable one (Köppen & Edmunds 1999) and that departures from equilibrium disappear with an e-folding timescale given by $M_g \ln(1/\mu)/\dot{M}_{\text{SFR}}$. Applying this timescale to UV-selected galaxies at $z \sim 2$, where by computing weighted means over bins 2–6 in Erb et al. 2006 we determine $(\langle \dot{M}_{\text{SFR}} \rangle, \langle M_g \rangle, \langle \mu \rangle) \approx (29 M_\odot \text{yr}^{-1}, 2.1 \times 10^{10} M_\odot, 0.38)$, we find that the timescale for y_{eff}/y to return to the closed-box yield is 700 Myr. This is considerably shorter than the gas consumption time of 1.2 Gyr. This short timescale together with the suppressed observed effective yields $y_{\text{eff}} < 0.01$ imply that star formation in these galaxies cannot be episodic in nature, consistent with the large inferred duty cycles. In our simulations, this timescale is less than 50% of the Hubble time at all epochs in both wind models, indicating that our predicted effective yields reflect star formation and gas accretion processes that are predominantly smooth rather than episodic in nature.

In summary, at high redshift ($z = 6 \rightarrow 2$) galaxies tend to evolve from high to low y_{eff} as accretion rates increase and are hence expected to “rebound” at lower redshifts $z < 2$ where gas accretion rates decrease. Superwind feedback generically suppresses y_{eff} in our galaxies as expected. The resulting $M_* - y_{\text{eff}}$ trend depends on the ways in which winds affect how inflows, outflows, and gas fractions scale with mass. The cw trend conflicts with high- and low-redshift observations while the vzw trend agrees qualitatively with low- but not all high-redshift observations. The fact that the vzw model produces better agreement with the directly-measured high- z MZR and low- z $M_* - y_{\text{eff}}$ trends suggests that our vzw model is closer to reality. In both cases star formation occurs via predominantly smooth rather than bursty processes. It will be interesting to see whether the vzw model’s conflict with the observed trend in y_{eff} at high- z is alleviated once direct measurements of gas densities at high redshifts become available.

6.3 Analytic Model MZR Evolution

In Section 7 we will synthesize the insights gained from our analytical model to understand the origin of the MZR in our simulations. In order to justify this analogy, in this section we show that our analytical model broadly reproduces the evolution of the simulated MZR.

Figure 12 compares how galaxies evolve through the MZR in our simulations (thin lines) versus our analytical model (thick lines) for three different mass bins. The analytical model succeeds in recovering most of the qualitative features of the models as well as the differences between them. For example, in each model the observable MZR has nonzero slope. This is only achieved if the star formation efficiency or the η_W scales with mass (Section 7.2). The agreement

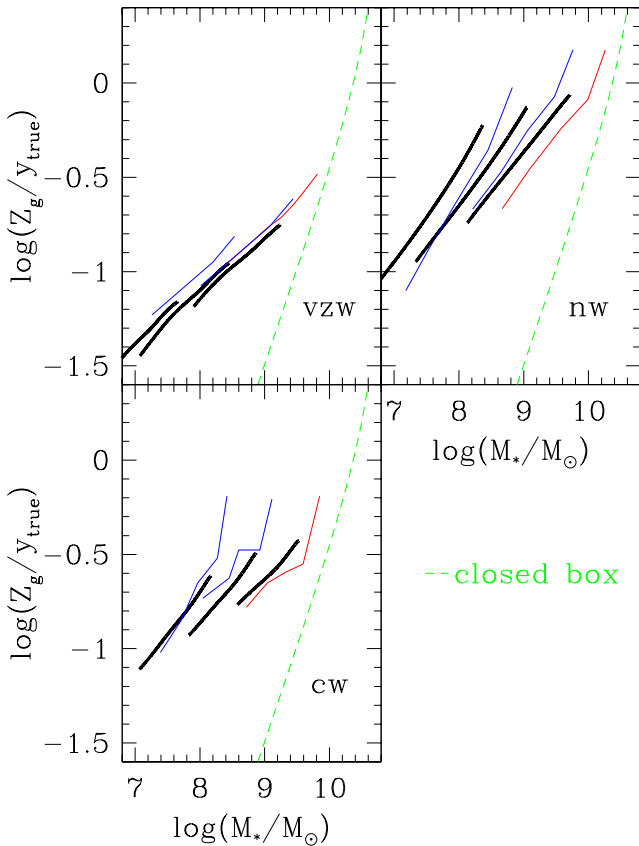


Figure 12. A comparison of the mean evolution of galaxies through the MZR in the w16 (thin blue) and w32 (thin red) models versus our analytical model. The analytical model reproduces the qualitative differences between the wind models although it does not reproduce the behavior of the individual models in detail. In particular, the analytical model yields a nonzero slope at low masses in the cw model, in clear conflict with the hydrodynamic simulations.

between the simulated and analytical trends results because we directly tuned our analytical star formation efficiencies to match Figure 5. We have verified that our analytic model reproduces the simulated galaxies’ effective yields as well (Figure 11) although we do not discuss it here.

The qualitative differences in evolution between our different outflow models are well-reproduced. For example, nw galaxies evolve the most from $z = 6 \rightarrow 2$ while cw galaxies evolve the least because the nw galaxies retain their entire gas reservoirs while the accretion histories in the cw model peak at an earlier time. The vzw galaxies evolve the most shallowly owing to their high η_W ’s while the nw galaxies evolve the most steeply. The result of these differences is that the vzw galaxies are the least enriched at $z = 2$ while the nw galaxies are the most enriched.

While our analytical model reproduces many of the gross features of the simulations as well as the differences between the different wind models, it does a poorer job of reproducing the individual wind models in detail. For example, in the nw and vzw models metallicities at $z = 2$ are ≈ 0.1 dex too low. Such offsets can easily result from minor inconsistencies in accretion histories or the definition of

the gas-phase metallicity. The upturn at late times is not conspicuous in any of our analytical models although it can readily be reproduced by forcing gas accretion rates to drop more precipitously at $z < 3$ than we have done. This is especially clear in the cw model, which is generally the most difficult model to reproduce owing to the fact that its behavior does not scale smoothly with galaxy mass. Our analytical cw model inevitably yields a nonzero slope in the observable MZR, in conflict with the simulations. This can be alleviated by allowing the star formation efficiencies \dot{M}_{SFR}/M_g to vary more slowly at low masses than at high masses (Figure 13). However, further fine-tuning of the star-formation efficiencies and accretion histories in our analytical model would yield little insight. The important point to take away from Figure 12 is that our analytical model captures the essential ingredients that determine how galaxies evolve through the MZR in our fully three-dimensional simulations. In the next Sections, we will therefore apply our analytical model to determine the conditions that drive the form of the observable MZR.

7 UNDERSTANDING THE MASS-METALLICITY RELATION

In this section we use the intuition gained in the past several sections along with the simulation results in order to piece together a comprehensive understanding of what drives the MZR’s form and evolution. We have already demonstrated that our vzw simulation produces good agreement with the slope, normalization, and scatter of the observed MZR (Figure 1) and that our analytical model provides an acceptable description of how galaxies evolve in our full simulation (Figure 12). Hence we begin by showing how our analytical model can account for the amplitude, slope, and scatter of the simulated—and, by implication, the observed—MZR.

7.1 Implications of the Model

7.1.1 Normalization and Scaling

Combining our original analytical model, equation 9, and the evolution of the gas mass, equation 13, it is straightforward to show that galaxies evolve through the MZR with a slope given by

$$\frac{d Z_g}{d M_*} = \frac{1}{M_g} \left(\frac{\dot{M}_{\text{ACC}}}{\dot{M}_{\text{SFR}}} Z_g (\alpha_Z - 1) + y \right), \quad (19)$$

which is equal to zero if

$$Z_g = y \frac{\dot{M}_{\text{SFR}}}{\dot{M}_{\text{ACC}}(1 - \alpha_Z)} \equiv Z_{g,\text{eq}} \quad (20)$$

This possible balance between the influences of star formation and infall has been identified previously (e.g., Tinsley & Larson 1978; Köppen & Edmunds 1999). Winds enter into the determination of $Z_{g,\text{eq}}$ indirectly by modulating the rate at which a galaxy depletes its gas reservoir as well as the relative enrichment of the satellite galaxies that it accretes. If a galaxy processes its gas into stars and winds

at the gas accretion rate¹, then $\dot{M}_{\text{SFR}}(1 + \eta_{\text{W}}) = \dot{M}_{\text{ACC}}$, which in turn yields the equilibrium gas-phase metallicity $Z_{g,\text{eq}} = y(1 + \eta_{\text{W}})^{-1}(1 - \alpha_{\text{Z}})^{-1}$. In what follows we will show that in our wind models this is approximately true.

7.1.2 Scatter

The ratio of a galaxy’s metallicity to its equilibrium metallicity $X_{\text{Z}} \equiv Z_{\text{g}}/Z_{g,\text{eq}}$ evolves with time according to

$$\frac{d X_{\text{Z}}}{d t} = \frac{\dot{M}_{\text{ACC}}}{M_{\text{g}}}(1 - X_{\text{Z}}) - y X_{\text{Z}} \left(\frac{\dot{M}_{\text{SFR}}}{\dot{M}_{\text{SFR}}} - \frac{\dot{M}_{\text{ACC}}}{\dot{M}_{\text{ACC}}} \right). \quad (21)$$

The second term in Equation 21 is small except during short-lived interactions, hence we may neglect it. In this case, Equation 21 implies that the equilibrium solution $X_{\text{Z}} = 1$ is a stable one (Köppen & Edmunds 1999) and that departures from equilibrium disappear on a timescale given by $M_{\text{g}}/\dot{M}_{\text{ACC}}$, or the timescale for the gas reservoir to be diluted by a factor of 2. If this timescale is shorter than the timescale over which perturbations to a galaxy’s metallicity occur then galaxies’ gas-phase metallicities recover from perturbations quickly, suppressing scatter in the observable MZR.

7.2 Normalization and Scaling Without Outflows

We begin our discussion of the origin of the MZR with the no-wind scenario in order to develop some intuition about how hierarchical structure formation impacts the MZR. In Figure 1 we showed that its MZR has approximately the correct slope, but an amplitude that is ≈ 0.5 dex too high. We further showed in Figure 6 that no-wind galaxies retain most of their gas, as expected without outflows. Hence the only physical effect left that can cause a slope in the MZR is the star formation efficiency.

If galaxies converted their gas into stars at precisely the gas accretion rate then the slope of the MZR in the nw model would be zero. This can be seen from the “infall model” formalism of Larson (1972), which tells us that if the gas mass is constant and $\dot{M}_{\text{SFR}} = \dot{M}_{\text{ACC}}$ then the gas metallicities evolve as:

$$\begin{aligned} Z_{\text{g}} &= y(1 - e^{-\nu}) \\ \nu &\equiv \mu^{-1} - 1, \end{aligned} \quad (22)$$

(Note that this can be obtained from Equation 19 by substituting $\dot{M}_{\text{SFR}}/\dot{M}_{\text{ACC}} = 1$.) In this model, for sufficiently small gas masses the MZR would be flat because the gas fraction μ would rapidly shrink to zero for all galaxies. Equivalently, Equation 21 tells us that we would expect all galaxies to approach $Z_{g,\text{eq}} = y$ as long as $M_{\text{g}}/\dot{M}_{\text{ACC}}$ were significantly less than the hubble time. The MZR clearly is not flat in the nw model. Therefore, guided by our discussion of Figure 7, we now ask whether the scaling of the star formation efficiency $\dot{M}_{\text{SFR}}/M_{\text{g}}$ can account for the scaling of the no-wind MZR.

We have calculated the $z = 2$ MZR using our analytical model with three different prescriptions for the SFR. In

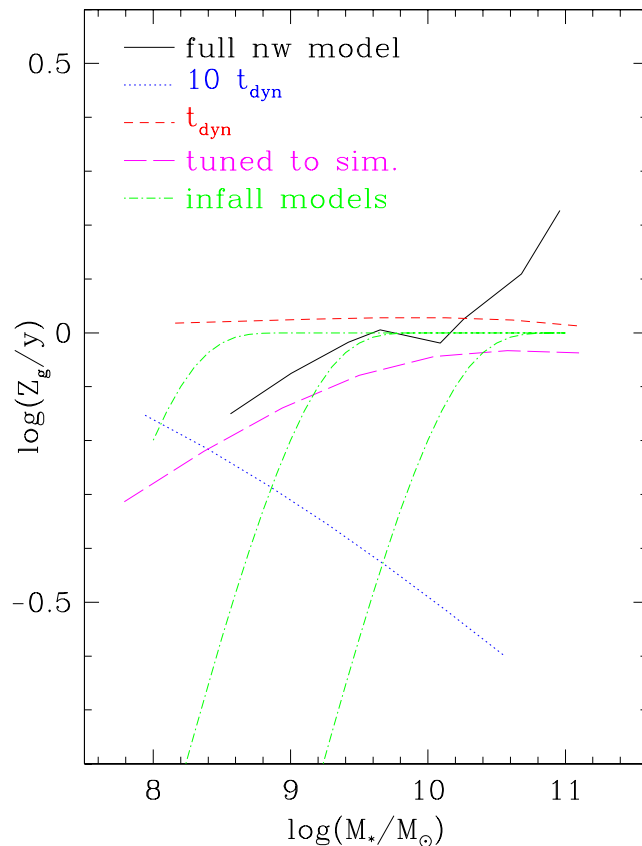


Figure 13. Predicted MZR at $z = 2$ in the nw model versus several analytical models. The solid black curve gives the mass-weighted gas-phase metallicity in the nw simulation. The red dashed and blue dotted lines are computed by assuming that gas collapses into stars in 1 and 10 dynamical times, respectively (see text); the long-dashed magenta line is computed by tuning star formation efficiencies to match the nw model. Green dot-dashed curves denote infall models (Equation 22) assuming constant gas masses of 10^8 , 10^9 , and $10^{10} M_{\odot}$ from left to right. The slope of the MZR in the absence of winds is dominated by the scaling of the star formation efficiency.

the first, we compute the star formation rate by assuming that gas condenses into stars in 10 dynamical times; this is similar to the Kennicutt (1998) relation. The gas densities are obtained from the baryonic masses by combining the Virial Theorem with the low-redshift baryonic Tully-Fisher relation (Geha et al. 2006) and assuming that galaxies are 5 times as dense as their host halos (the value chosen for this ratio affects the amplitude but not the trend of our results). In the second, we assume that gas condenses into stars in one dynamical time. In the third, we tune the star formation efficiencies $\dot{M}_{\text{SFR}}/M_{\text{g}}$ to reproduce the efficiencies in the nw simulations.

Figure 13 compares the resulting MZR at $z = 2$ with the trend from the fully three-dimensional nw model using mass-weighted gas-phase metallicities (solid black curve). Additionally, we have plotted the evolution of Z_{g} versus $M_{\text{*}}$ for three representative infall models (Equation 22; green dot-dashed curves) corresponding to constant gas masses of 10^8 , 10^9 , and $10^{10} M_{\odot}$ from left to right. The trend from

¹ This can be viewed as setting the constant $k \equiv \dot{M}_{\text{SFR}}/\dot{M}_{\text{ACC}}$ in Tinsley & Larson (1978).

the 10-dynamical time prescription has a negative slope, indicating that more massive galaxies possess larger gas masses (and larger gas fractions) than less massive galaxies and hence cannot enrich their gas reservoirs as effectively; in terms of Equation 19, since $\dot{M}_{\text{SFR}}/\dot{M}_{\text{ACC}}$ declines with increasing M_* , Z_g does as well. The trend from the one dynamical time model is flat, as expected for a scenario with such efficient star formation; indeed, for this model $\dot{M}_{\text{SFR}} \approx \dot{M}_{\text{ACC}}$ so that Equation 22 accurately predicts $Z_g/y = 1$ for all masses since the gas fractions are negligible. By contrast, the trend from the model in which we have tuned the star formation efficiencies exhibits the desired positive slope. This trend is in qualitative agreement with the numerical trend although the most massive nw galaxies exhibit metallicities above the yield. The high metallicities at the massive end are likely a consequence of accreting pre-enriched gas; in terms of Equation 19, $\alpha_Z > 0$.

The simulated trend is shallower than expected from Equation 22 because the assumption $\dot{M}_{\text{SFR}} = \dot{M}_{\text{ACC}}$ is violated weakly in the absence of outflows; in particular, $\dot{M}_{\text{SFR}}/\dot{M}_{\text{ACC}}$ drops from 1.0 at $10^8 M_\odot$ to 0.9 at $10^{11} M_\odot$ in the analytical (magenta) curve while μ drops from 0.6 to 0.2 over the same interval. In short, the reason the nw model has the correct MZR slope is that the star formation efficiency in a hierarchical structure formation scenario naturally yields the desired differential with galaxy mass (cf. § 5.2). Nevertheless, the excessive amplitude (cf. Figure 1) suggests that metals must be preferentially removed from these galaxies. Hence outflows are necessary to obtain the correct amplitude (Kobayashi et al. 2007), but are *not* required to obtain the suppression of metallicity in low-mass galaxies (De Rossi et al. 2006; Tassis et al. 2006).

7.3 Normalization and Scaling With Outflows

Next we consider the impact of winds. From Figure 9 we see that outflows suppress both the stellar mass and the metallicity. In order to lower the MZR amplitude, outflows must lower Z_g more than $M_*^{-0.3}$, which is the observed slope of the MZR.

Looking first at $M_* = 10^{10} M_\odot$, which is around L_* at $z = 2$, we see from Figure 1 that both the cw and vzw models produce roughly the correct MZR amplitude (recall that the observed metallicities and the yield each introduce ≈ 0.3 dex of uncertainty). Under the assumption that the MZR is governed primarily by the mass loading factor η_W via the equilibrium conditions (cf. § 7.1.1), this is expected because galaxies in both models experience effective mass loading factors in the range $\tilde{\eta}_{\text{MLF}} = 1 - 1.5$ at this scale (cf. Figure 6). Intuitively, $\tilde{\eta}_{\text{MLF}}$ determines the level of suppression of gas enrichment and stellar mass growth because higher mass-loading factors lead to lower gas densities (cf. Figure 5) and to more gas being ejected in winds rather than converted into stars. This leads to a tendency for galaxies with similar $\tilde{\eta}_{\text{MLF}}$ to possess similar properties regardless of wind model.

Above this mass scale, constant wind outflows cannot escape halos, causing $\tilde{\eta}_{\text{MLF}}$ to drop rapidly. Hence cw metallicities grow much more rapidly with M_* than observed. Below this scale, metallicities reach a minimum in the range $M_* = 10^{9.5} M_\odot$ and then “rebound” slightly to lower masses. If this trend continues to $z = 0$ (as it does from $z \approx 6 \rightarrow 2$),

then this would be in gross conflict with observations. The cause of this scaling likely owes to the flat trend of $\tilde{\eta}_{\text{MLF}}$ with mass at low masses, with the slight rebound at low masses due to baryon stripping from nearby galaxies’ outflows as discussed before (see also Scannapieco & Broadhurst 2001, Figure 12).

In the vzw case, galaxies are always below the blowout scale (which increases linearly with mass). In this regime, the mass loading factor governs the MZR. In order for the scaling of $Z_g \propto M_*^{0.3}$ to hold, η_W must be roughly proportional to $M_*^{-0.3}$, which is satisfied in the vzw case. There is also slight evidence for baryon stripping, but it is highly subdominant compared to the high $\tilde{\eta}_{\text{MLF}}$ in the mass range where stripping is effective.

In summary, winds suppress galaxy masses and metallicities primarily by modulating the relative rates at which gas reservoirs are enriched and diluted and secondarily by stripping baryons from neighboring galaxies. In the vzw model the latter effect is small compared to the former while in the cw model both are significant. We emphasize that the normalization and scaling of the MZR are *not* determined by the total fraction of metals that galaxies retain because the rates of gas accretion and star formation are too rapid for the gas reservoirs to retain any memory of this quantity. If baryon stripping is negligible compared to the effects of outflows then the most important parameter is the effective mass loading factor $\tilde{\eta}_{\text{MLF}}$; if the wind speed exceeds the escape velocity then $\tilde{\eta}_{\text{MLF}} \propto \eta_W$ and the scaling of η_W dominates the MZR.

7.4 Normalization and Scaling: The Equilibrium Metallicity

We now illustrate our main result that the mass loading factor governs the MZR below the blowout scale by applying the analytical relations derived in § 7.1 to the vzw simulation. In particular, we show that our simulated galaxies’ metallicities do indeed track the equilibrium metallicity.

For each simulated galaxy in the vzw model, we have used our progenitor lists to track how the ratio of its gas phase metallicity to its equilibrium metallicity ($X_Z \equiv Z_g/(y\dot{M}_{\text{SFR}}/\dot{M}_{\text{ACC}})$; cf. Section 7.1.2) varies with mass and time during the interval $6 < z < 2$. If galaxies’ gas-phase metallicities closely track equilibrium and if infalling material is unenriched then we expect $X_Z \approx 1$ at all masses and redshifts.

The result is shown in the top panel of Figure 14. Comparing the least and most massive galaxy bins, we find that whereas the actual gas metallicities of $10^{10.8} M_\odot$ and $10^{8.7} M_\odot$ galaxies differ by ≈ 0.6 dex at $z = 2$ (Figure 1), their X_Z ’s only differ by ≈ 0.2 dex. Moreover, the spread in X_Z is even tighter before $z = 2$. This would not be expected in the absence of an equilibrium condition. The fact that the spread in these ratios is tighter than the spread in galaxies’ actual metallicities indicates that at all times galaxies’ metallicities are tightly constrained by a balance between enrichment from star formation and dilution from inflows. The fact that the ratios are offset from zero implies that the mean metallicity of inflowing gas is more than 10% of the mean metallicity in the galaxy’s ISM and reflects the widespread presence of galactic fountains in the vzw model; the ratio α_Z can be read from the y-axis on the right side

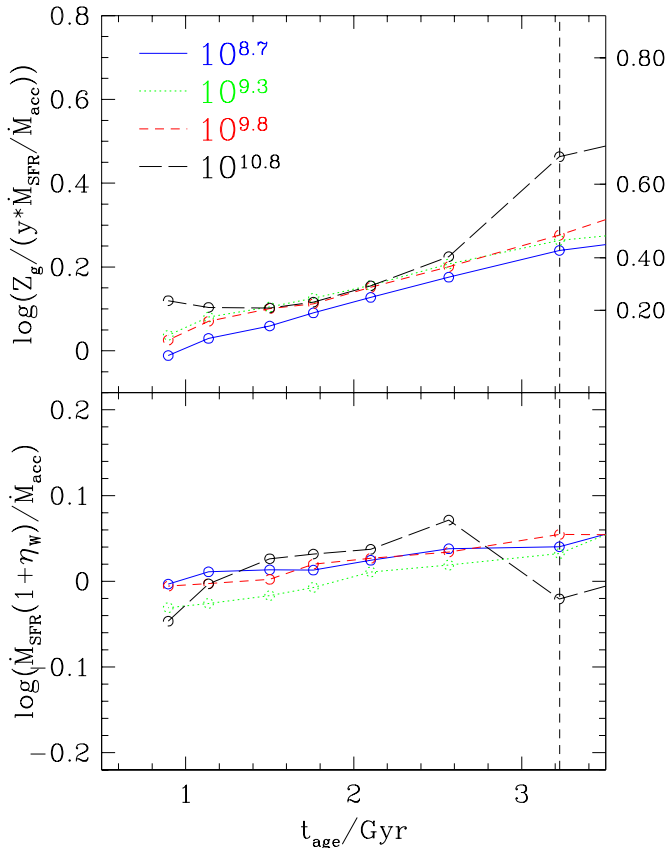


Figure 14. (Top) Mean ratio of actual to equilibrium gas-phase metallicity in four bins of M_* in the vzw model. The different curves correspond to galaxies in different mass bins; the legend gives the stellar masses at $z = 2$. The vertical dashed line denotes $z = 2$. (Bottom) Mean ratio of the gas processing to gas accretion rates. The mean metallicity of infalling material grows with both galaxy mass and time and is roughly $\alpha_Z = 50\%$ of the mean ISM metallicity at $z = 2$ (right y-axis on top panel). Gas processing rates generally lie within 20% of the equilibrium values at all times.

of the top panel. The increase in α_Z with cosmic time reflects the growing relative contribution of galactic fountain gas with respect to pristine ISM gas: by $z = 2$, $\alpha_Z \approx 50\%$, indicating that roughly 50% of the infalling gas is galactic fountain material. The increase in α_Z with mass reflects the fact that the rate at which pristine IGM gas accretes onto the galaxies declines with increasing halo mass owing to their increasing hot gas fractions (e.g., Birnboim et al. 2007).

The top panel of Figure 14 also supports our view that pre-enrichment of gas that falls onto galaxies is not significant in the vzw simulation, which can be understood as follows: If, at a given redshift, gas that is being accreted were homogeneously pre-enriched to a certain level, this pre-enrichment would provide a relatively larger boost to the metallicities of low-mass galaxies than to massive galaxies. As a result, the gas-phase metallicities of low-mass galaxies would lie farther above their expected equilibrium value given unenriched infall, and the normalization of the X_Z trend for low-mass galaxies would be boosted systematically above the X_Z trend for more massive galaxies. In fact, all

but the most massive galaxies display roughly the same ratio X_Z down to $z = 2$, hence a homogeneous pre-enrichment is not significant in this model.

In Sections 6 and 7 we proposed that the rate at which gas is processed into stars and winds tracks the rate at which it is accreted, $\dot{M}_{\text{SFR}}(1 + \eta_w) = \dot{M}_{\text{ACC}}$. This idea is central to the current work as it allows us to demonstrate that the slope and normalization of the MZR depend almost entirely on the scaling of η_w . Additionally, a systematic imbalance between the rates of gas accretion and gas processing could in principle mimic the effects of nonzero α_Z , leading to an incorrect interpretation of the top panel of Figure 14. For this reason, we show the ratio of the gas processing to the gas accretion rates in our vzw model in the bottom panel of Figure 14. This figure indicates that galaxies generally process their gas at the same rate as they accrete it, justifying our assumption² that $\dot{M}_{\text{SFR}}/\dot{M}_{\text{ACC}} = 1/(1 + \eta_w)$ and supporting our view that the increase in X_Z with time in the top panel results from galactic fountains rather than a mismatch between gas accretion and gas processing rates. Interestingly, this plot also indicates that, in the vzw model, mergers do not contribute significantly to the buildup of galaxies’ stellar populations even in our most massive bin. Because we measure baryonic accretion rates rather than strict gas accretion rates (the latter being difficult to infer from our simulations), a tendency for galaxies to accrete a significant fraction of their baryons as ready-formed stars would show up as a tendency for the accretion rate to exceed the gas processing rate. There is some evidence that this does occur in the most massive galaxies in the vzw model, i.e. that dry mergers are more prevalent at high masses. However, on average galaxies at $z \geq 2$ do not accrete more than $\approx 10\%$ of their baryons in the form of already-formed stars (see also Guo & White 2007).

In summary, the top panel of Figure 14 verifies that the slope and normalization of the observable MZR are dominated by the equilibrium condition in Equation 20, while the bottom panel verifies that galaxies process newly accreted gas into stars and winds at roughly the gas accretion rate. In other words, at all masses and redshifts, metallicities are dominated by an equilibrium between the rates of enrichment and dilution while the enrichment rate is dominated by an equilibrium between the rates of gas accretion and gas processing. These equilibrium rates are governed primarily by the mass loading factor, hence the scaling of the mass loading factor directly determines the scaling of the MZR.

7.5 Scatter

In our analytical model, scatter in the MZR occurs because a perturbation, such as an accretion or merger event, displaces a galaxy’s metallicity from its equilibrium value. The timescale to return to equilibrium is given by the gas dilution time M_g/\dot{M}_{ACC} . Perturbations to a galaxy’s metallicity are expected to occur on timescales no shorter than the dynamical time, $t_{\text{vir}} \simeq 2.5\text{Gyr}/(1+z)^{3/2}$. Hence if the dilution time is shorter than the dynamical time, then we expect pertur-

² Note that this is a generalization of the *Ansatz* $\dot{M}_{\text{SFR}} = \dot{M}_{\text{ACC}}$ that was introduced by Larson (1972).

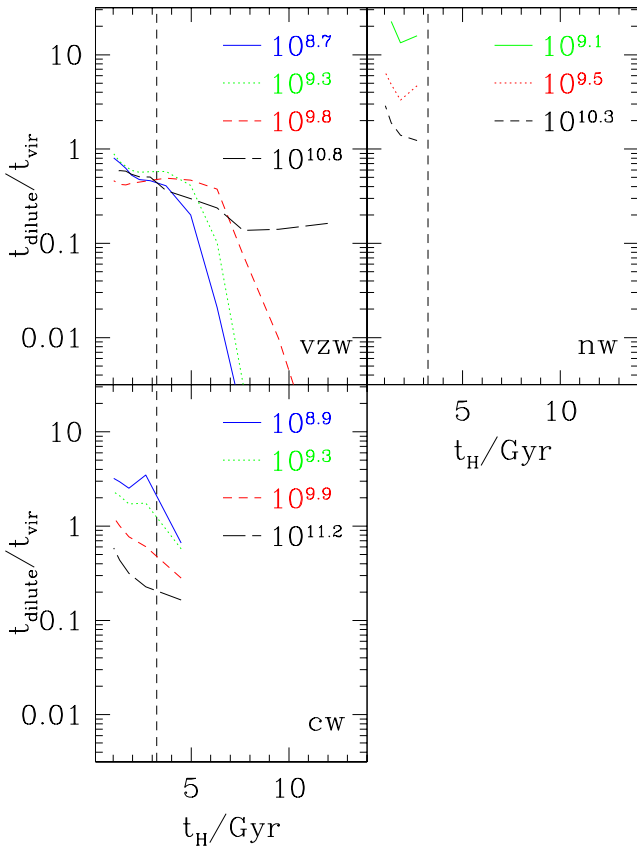


Figure 15. The ratio of the dilution time M_g/\dot{M}_{ACC} to the dynamical time as a function of mass and time in our various models. The galaxy masses at $z = 2$ are indicated in the legend and the vertical dashed lines indicate $z = 2$. Comparison with Figure 1 indicates that mass scales with short dilution times tend to show small scatter in the MZR whereas mass scales with long dilution times tend to show large scatter.

bations to disappear rapidly and for the scatter in the MZR to be tight.

Figure 15 shows how the ratio of the dilution time to the dynamical time varies with scale and time in our models. In the nw models the dilution times scale inversely with mass at early times from roughly $1.5t_{\text{vir}}$ in the most massive galaxies to roughly $15t_{\text{vir}}$ in the lowest-mass galaxies at $z \sim 2-3$. In the cw model the dilution time scales more slowly with mass although the trend for low-mass galaxies to dilute their gas reservoirs more slowly than massive galaxies is preserved despite the cw winds. Generally, galaxies less massive than $10^{10}M_{\odot}$ have dilution times longer than t_{vir} at $z = 2$ while more massive galaxies have dilution times that are shorter than t_{vir} . Finally, in the vzw model the dilution time does not exceed t_{vir} at any mass scale. More interestingly, in this model it is the low-mass galaxies whose dilution times are the shortest, a direct consequence of our assumption that the mass loading factor scales with the inverse of the velocity dispersion.

Turning to the question of the scatter in the MZR (Figure 1), the relatively long dilution times in the nw model at $z = 2$ are consistent with the relatively large scatter (≈ 0.11

dex) in the corresponding MZR: Because perturbations to these galaxies’ metallicities disappear relatively slowly, they spend a relatively large amount of time out of equilibrium. Galaxies in the vzw model possess significantly shorter dilution times than the nw galaxies or the low-mass cw galaxies, consistent with the tight scatter (≈ 0.08 dex) in the vzw MZR at all scales. In the cw model low-mass galaxies possess long dilution times and large scatter whereas massive galaxies possess short dilution times and small scatter, as expected. The most massive cw galaxies possess the shortest dilution times of any of our simulated galaxies at $z = 2$, consistent with the extremely tight scatter (≈ 0.06 dex) in the cw MZR above the blowout scale. The dilution times for low-mass cw galaxies are shorter than they are for the low-mass nw galaxies even though the scatter in the MZR is largest for the low-mass cw galaxies. The extra scatter at low masses owes to these galaxies having had their baryons stripped by winds from neighboring galaxies. Because the amount of stripping varies with environment, it effectively creates a range of equilibrium metallicities for each halo mass.

In summary, galaxies tend to process gas into stars and winds at roughly the gas accretion rate. This tendency leads to the existence of an equilibrium gas-phase metallicity $Z_{g,\text{eq}} = y\dot{M}_{\text{SFR}}/\dot{M}_{\text{ACC}}$, which encodes information regarding both a galaxy’s present conditions (via the accretion rate and wind properties) and its star formation history (via the current gas content, which determines \dot{M}_{SFR}). Corrections to this zeroth-order equilibrium result from galaxies accreting pre-enriched gas or ready-formed stars as well as effects that depend on environment; the first two of these effects should not increase the scatter in the MZR while the last one should. Metallicities are expected to lie close to $Z_{g,\text{eq}}$ as long as dilution times are short compared to a dynamical time; in our momentum-driven wind model that achieves the best agreement with the observed $z = 2$ MZR, this holds for all scales and epochs. Our interpretation of the origin of the MZR scatter also explains the no-wind and constant wind cases. Together with its relative simplicity, we believe this makes our interpretation reasonably compelling.

8 SUMMARY

In this paper we have compared the observed MZR of star-forming galaxies at $z \sim 2$ with predictions from cosmological hydrodynamic simulations that incorporate three different models for galactic outflows: No outflows, a “constant wind” model that emulates the energy-driven Dekel & Silk (1986) scenario, and a “momentum-driven wind” model that reproduces $z \gtrsim 2$ IGM metallicity observations (Oppenheimer & Davé 2006). We have shown that the momentum-driven wind model produces the best agreement with the slope, normalization, and scatter of the observed MZR. We have constructed a simple analytical model that qualitatively reproduces the behavior of our simulations, and used it to identify the processes that drive galaxies’ metallicities. Our work shows that the slope, normalization, and scatter of the MZR as well as its evolution with time all constitute constraints on the behavior of outflows. In particular, our simulations strongly disfavor any constant wind scenario, and explain why our momentum-driven wind model produces reasonable agree-

ment with available constraints. Our main conclusions are summarized as follows:

- Outflows are required in order to bring the simulated and observed MZR into agreement at $z \approx 2$. Without outflows, enrichment proceeds too rapidly relative to dilution with the result that galaxy metallicities are 2–3 \times higher than observed.

- The MZR is governed by an evolving equilibrium between the enrichment rate owing to star formation and the dilution rate owing to gas accretion. This results in an *equilibrium metallicity* for any given galaxy, given by $Z_{g,\text{eq}} = y\dot{M}_{\text{SFR}}/\dot{M}_{\text{ACC}}$, where y is the yield, \dot{M}_{SFR} is the star formation rate, and \dot{M}_{ACC} is the gas accretion rate.

- Outflows affect $Z_{g,\text{eq}}$, and hence the MZR, by limiting the gas supply for star formation. For a given mass loading factor η_{W} , and assuming (as our simulations predict) infalling gas has a negligible metallicity, then $Z_{g,\text{eq}} = y/(1 + \eta_{\text{W}})$.

- Wind speeds (V_{W}) affect the MZR by governing how much outflowing mass actually escapes the halo. This results in an effective mass loading parameter $\tilde{\eta}_{\text{MLF}}$ (Figure 6), which is similar to (but slightly less than) η_{W} so long as winds are fast enough to escape a galaxy’s halo, and drops rapidly towards zero for galaxies whose winds are slower than the escape speed. Our simulations’ metallicities are hence well described by $Z_{g,\text{eq}} \approx y/(1 + \tilde{\eta}_{\text{MLF}})$, where $\tilde{\eta}_{\text{MLF}} \approx \eta_{\text{W}}$ below the blowout scale, and $\tilde{\eta}_{\text{MLF}} \approx 0$ above it.

- The reheating scale, which is the mass below which the outflow energy input is sufficient to unbind all the gas, does not play a significant role in determining $\tilde{\eta}_{\text{MLF}}$. This is evident because in our cw run the fraction of baryons converted to stars (f_*) does not vary with halo mass in the way expected under the assumption of efficient energetic coupling of outflows with ambient gas (Figure 7). Physically, this is because in our simulations outflows tend to blow holes in surrounding gas rather than heat it.

- The observed slope and amplitude of the MZR therefore constrain how $\tilde{\eta}_{\text{MLF}}$ and V_{W} varies with M_* . Our momentum-driven wind model obtains the observed relation $Z_g(M_*) \propto M_*^{0.3}$ by having $\eta_{\text{W}} \propto 1/\sigma \propto M_{\text{halo}}^{-1/3} \propto M_*^{-1/3}$, and by having outflow speeds always above the escape velocity (so $\tilde{\eta}_{\text{MLF}} \approx \eta_{\text{W}}$). The latter constraint requires some positive mass dependence of outflow speeds on galaxy mass, which we assumed to be $V_{\text{W}} \propto \sigma$, but any dependence where galaxy masses are always below the blowout scale would suffice.

- Our no-wind scenario also produces a MZR with roughly the correct slope, though in detail it is too shallow. In the absence of outflows, this owes to a mass dependence of M_* on M_{halo} such that low-mass galaxies have a lower fraction of baryons in stars. Hence in principle it is possible to match the observed MZR without having $\tilde{\eta}_{\text{MLF}}$ vary with M_* . However, the required scaling of M_* with M_{halo} does not occur naturally in our simulations with outflows.

- Our constant wind scenario fails to even qualitatively match the observed MZR. The existence of a blowout scale at $\sim 10^{10} M_{\odot}$ produces a marked feature in the MZR, below which $\tilde{\eta}_{\text{MLF}} \approx \eta_{\text{W}} = \text{constant}$, and above which $\tilde{\eta}_{\text{MLF}}$ goes rapidly to zero and hence the MZR rises quickly towards $Z_{g,\text{eq}} = y$. Such a feature is generically expected across the

blowout scale. The absence of such a feature in the observed $z \approx 0$ MZR from $M_* \approx 10^7 - 10^{11} M_{\odot}$ argues against a blowout scale in that mass range, thereby ruling out any reasonable constant wind speed scenario.

- The scatter in the MZR is governed primarily by the dilution time $t_{\text{d}} = M_g/\dot{M}_{\text{ACC}}$ compared to the dynamical time t_{vir} . If dilution times are short compared to a dynamical time, then perturbations from $Z_{g,\text{eq}}$ have time to equilibrate, thereby suppressing scatter. The small scatter seen in the MZR argues for $t_{\text{d}}/t_{\text{vir}} \lesssim 1$ across the full range of observed masses. Our momentum-driven wind model satisfies this non-trivial constraint, whereas our other models do not (Figure 15).

- Another physical effect that plays a secondary role in governing the MZR is that outflows carry significant amounts of momentum that can strip baryons from neighboring halos. This increases scatter by causing equilibrium metallicities to depend on environment as well as mass. Hence the tight scatter in the observed MZR suggests that either galactic winds do not carry significant amounts of momentum out of galaxies, or outflows must be sufficiently mass-loaded to “drown out” the effects of baryonic stripping. In our constant wind case below the blowout scale, neither are true, and the scatter increases significantly. In our momentum-driven wind case, the latter is generally true.

- Outflows and inflows cause galaxies to evolve more shallowly than closed-box models at early times, with the vzw galaxies evolving most shallowly of all (Figure 11). Effective yields are expected to be ~ 0.01 at $z = 2$ for both our wind models. However, the detailed scaling of the vzw model’s y_{eff} suggests better agreement with the well-constrained low-redshift observations. It is worth noting that the effective yield is only reflective of the recent history of gas and metal accretion over a dilution time, hence it cannot be used to infer long-term accretion histories.

According to our analysis, an outflow model that will successfully reproduce the observed MZR must satisfy three main conditions:

- (i) $\eta_{\text{W}} \propto (\text{slope of MZR})^{-1}$ when $\eta_{\text{W}} \gg 1$;
- (ii) V_{W} must scale with mass such that all galaxies are below the blowout scale (so that $\tilde{\eta}_{\text{MLF}} \approx \eta_{\text{W}}$);
- (iii) Dilution times must be short compared to dynamical times in order to maintain a small MZR scatter at all masses.

These criteria show that the MZR mostly constrains the mass loading factor, with weaker constraints on outflow speeds and gas accretion rates. It is interesting that our momentum-driven wind scenario naturally satisfies these requirements (along with secondary requirements such as the subdominance of baryon stripping). Although other wind models could conceivably be postulated that also satisfy these requirements, it is compelling that this same model also satisfies IGM metallicity constraints, and broadly agrees with available direct measurements of outflow parameters at high and low redshift. In any case, other wind models will likely need to satisfy the above criteria in order to match the observed MZR, demonstrating that the MZR provides strong constraints on outflow properties.

The rather dramatic failure of our constant wind scenario is surprising in light of the apparent success of the simple analytical models presented by Dekel & Silk (1986)

and Dekel & Woo (2003). The root difference traces back to those works assuming that feedback suppresses star formation by efficiently coupling supernova energy with baryons in halos, while our three-dimensional simulations produce inefficient coupling with a propensity for winds to blow holes in surrounding gas. This is partly a result of the way we implement winds in our simulations by turning off hydro forces for some distance; however, in practice that distance is much smaller than the halo size and hence interactions with halo gas can (and do) still occur. Regardless, the existence of a strong feature at the blowout scale seems an unavoidable consequence in a constant wind scenario, and is in direct conflict with the observed unbroken MZR power law over four orders of magnitude in stellar mass. Furthermore, the increased scatter below the blowout scale predicted by such a scenario is not seen. Hence we strongly disfavor this explanation of the MZR.

The slow turnover in the $z \sim 0$ MZR at $M_* \gtrsim 10^{10.5} M_\odot$ cannot be studied directly in our simulations owing to a lack of sufficient dynamic range, along with the fact that our simulations were not evolved to $z = 0$. However, it arises naturally in our scenario when the mass loading factor becomes $\ll 1$, which yields $Z_{g,\text{eq}} \rightarrow y = \text{constant}$. In principle, it could also arise if galaxies with $M_* \gtrsim 10^{10.5} M_\odot$ are above the blowout scale (which would also make $\tilde{\eta}_{\text{MLF}} \rightarrow 0$); indeed, this is the conventional interpretation (e.g. Tremonti et al. 2004). However, this would imply the existence of a blowout scale at that mass, which as we have argued above causes other features in the MZR that contradict observations. Hence we suggest that this mass scale does not reflect a characteristic wind speed, but rather a characteristic scale of the mass loading factor, namely the galaxy mass where the mass loading factor is roughly unity.

Our findings agree broadly with those from the higher-resolution study of Brooks et al. (2006), though there are some differences in interpretation. In their work, they determined that winds affect the MZR of low-mass galaxies in the following sense: When they compared gas-phase metallicities at $z = 0$ with the mean metallicity of all gas that had ever belonged to the galaxies, they found no systematic offset. This is expected if the mean metallicity in an outflow equals the mean metallicity in the galaxy’s ISM. On the other hand, by comparing simulations with and without winds they found that winds suppress gas densities and hence star formation efficiencies, which in turn shapes the observable MZR. Hence they deduced that star formation efficiency is a key driver of the MZR. We also find that more massive galaxies have more efficient star formation in Figure 5, and Figure 13 shows that this is important for establishing the MZR, at least in the no-wind case.

However, in our wind models we find that the star formation efficiency doesn’t by itself determine the MZR, because the trends in Figure 7 don’t mimic those of the MZR. Instead, the MZR’s trend is the mass scaling of $Z_{g,\text{eq}}$, which is set by how the accretion rate compares with the star formation rate (Tinsley & Larson 1978; eqn. 20); in our models, this is similar across all masses and close to unity at $z \sim 2$, when the dependence on η_{W} is taken into account, as shown in the bottom panel of Figure 14. Hence the mass dependence in $Z_{g,\text{eq}}$ arises mainly from the mass dependence in $\tilde{\eta}_{\text{MLF}}$. In this way, the trends in $\tilde{\eta}_{\text{MLF}}$ (Figure 6) are directly reflected in the MZR.

This interpretation can be compared with the results of Kobayashi et al. (2007), who observed a tight correlation between stellar metallicity and the mass fraction of metals retained by the galaxies in their models at all redshifts (their Figure 16d) and concluded that higher stellar metallicities result directly from a lower mass fraction of metals ejected. Our models obey a similar correlation, hence our conclusions should be consistent with theirs. In fact, the tendency of gas-phase metallicities to track an equilibrium value combined with a tendency for $\tilde{\eta}_{\text{MLF}}$ to decline and $Z_{g,\text{eq}}$ to grow as galaxies grow *requires* that the fraction of metals retained and the mean stellar metallicity must grow together, as found by Kobayashi et al. (2007). Moreover, given that the gas-phase MZR shows little scatter at all redshifts, the stellar MZR should also show little scatter (as also noted by Kobayashi et al. 2007) even though it is not directly governed by an equilibrium condition analogous to Equation 20. In this way, Equation 20 likely governs the gas-phase MZR directly and the stellar MZR indirectly in both sets of models. Indeed, it is likely that an analogous equilibrium condition governs the MZR of *any* galaxy evolution model that incorporates a treatment for strong ($\tilde{\eta}_{\text{MLF}} \gg 1$) outflows.

Despite considerable progress over the last decade, the use of metallicities and effective yields to constrain galaxy evolution constitutes a field that is in its infancy from both theoretical and observational perspectives. Our simulations’ implementation of outflows, while being state-of-the-art for cosmological simulations, is still crude. For instance, we currently assume enrichment only from Type II supernovae, we do not shut off winds in galaxies with low star formation rate surface densities (Heckman 2003), and we use the local potential as a proxy for galaxy mass. All of these simplifications are probably not fatal at $z = 2$, but by $z = 0$ they likely are; this (in addition to computer time constraints) is the main reason we have not attempted to extend our simulation analysis to $z = 0$. We are working towards incorporating metals from Type Ia supernovae and stellar mass loss, improved wind criteria, and direct galaxy identification into our code (Oppenheimer et al., in preparation). Our preliminary results indicate that none of these issues significantly impact the predicted $z = 2$ MZR.

Another aspect for future exploration is different scalings of the wind model. For instance, our constant wind scenario is only one possible implementation of energy-driven outflows. More sophisticated versions that allow η_{W} and the wind speed to vary could improve the agreement between the observed and simulated luminosity functions at the faint end while yielding agreement with the observed MZR. It is by no means clear that momentum-driven winds, as we have implemented them, are the only viable alternative. Indeed, it is for this reason intriguing that Kobayashi et al. (2007) have obtained reasonable agreement with the observed MZR using a treatment for *pressure*-driven outflows that result in a qualitatively similar scaling of mass-loading factor versus mass as well as the predicted MZR. The intuition gained from these results can hopefully guide us (and others) towards understanding how alternative outflow models may fare prior to running expensive simulations.

On the observational side, galactic outflows are still relatively poorly constrained despite impressive advances over the past decade. More detailed measurements of the mass

loading factors and wind speeds across a large dynamic range would be helpful in indicating whether momentum-driven or energy-driven winds are likely to dominate. More importantly, despite heroic observational efforts there remain relatively few constraints on galaxies' metallicities and gas fractions at high redshift. Upcoming metallicity measurements made with multi-object infrared spectrographs such as FLAMINGOS-2 as well as direct gas mass measurements made with IRAM and ALMA will prove crucial in finally allowing us to apply these metrics to the high-redshift Universe.

Despite its simplicity, the fact that our model explains the detailed shapes of both of our wind models' MZR leads us to believe that it captures most of the essential physics. Our scenario invokes two parameters, the equilibrium metallicity and the dilution time, neither of which can be directly measured because they depend on the gas accretion rate. Instead, they must be constrained indirectly through observations of how galaxy properties such as SFR, gas mass, and metallicity vary with mass and epoch. We look forward to undertaking such comparisons to observations in the future, and are hopeful that they will shed further light on the critical problem of understanding galactic outflows.

ACKNOWLEDGEMENTS

We thank V. Springel and L. Hernquist for providing us with Gadget-2. We thank Christy Tremonti, Don Garnett, John Moustakas, Alison Coil, Nicolas Bouché, Ben Oppenheimer, and Daniel Eisenstein for assistance and helpful discussions. We thank the anonymous referee for many helpful comments that improved the paper. Partial support for this work was provided by NASA through grant numbers HST-AR-10647 and HST-AR-10946 from the Space Telescope Science Institute, which is operated by the Association of Universities for Research in Astronomy, Inc., under NASA contract NAS5-26555. Partial support for this work, part of the Spitzer Space Telescope Theoretical Research Program, was provided by NASA through a contract issued by the Jet Propulsion Laboratory, California Institute of Technology under a contract with NASA. Our simulations were run on the Xeon Linux Supercluster at the National Center for Supercomputing Applications. KMF acknowledges support from a National Science Foundation Graduate Research Fellowship.

REFERENCES

- Adelberger, K. L., Steidel, C. C., Pettini, M., Shapley, A. E., Reddy, N. A., & Erb, D. K. 2005, *ApJ*, 619, 697
- Adelberger, K. L., Shapley, A. E., Steidel, C. C., Pettini, M., Erb, D. K., & Reddy, N. A. 2005, *ApJ*, 629, 636
- Adelberger, K. L., Steidel, C. C., Shapley, A. E., & Pettini, M. 2003, *ApJ*, 584, 45
- Baker, A. J., Tacconi, L. J., Genzel, R., Lehnert, M. D., & Lutz, D. 2004, *ApJ*, 604, 125
- Yee, H. K. C., Ellingson, E., Bechtold, J., Carlberg, R. G., & Cuillandre, J.-C. 1996, *AJ*, 111, 1783
- Berger, E., et al. 2007, *ApJ*, 665, 102
- Birnboim, Y., Dekel, A., & Neistein, E. 2007, *MNRAS*, 380, 339
- Bouché, N., Lehnert, M. D., & Péroux, C. 2005, *MNRAS*, 364, 319
- Bouché, N., et al. 2007, in prep
- Brooks, A. M., Governato, F., Booth, C. M., Willman, B., Gardner, J. P., Wadsley, J., Stinson, G., & Quinn, T. 2007, *ApJL*, 655, L17
- Chabrier, G. 2003, *PASP*, 115, 763
- Chieffi, A., & Limongi, M. 2004, *ApJ*, 608, 405
- Dalcanton, J. J. 2007, *ApJ*, 658, 941
- Davé, R., Finlator, K., & Oppenheimer, B. D. 2006, *MNRAS*, 370, 273
- Davé, R., Finlator, K., & Oppenheimer, B. D. 2006, *astro-ph/0608537*
- Davé, R., & Oppenheimer, B. D. 2007, *MNRAS*, 374, 427
- Dekel, A., & Silk, J. 1986, *ApJ*, 303, 39
- Dekel, A., & Woo, J. 2003, *MNRAS*, 344, 1131
- De Lucia, G., Kauffmann, G., & White, S. D. M. 2004, *MNRAS*, 349, 1101
- de Rossi, M. E., Tissera, P. B., & Scannapieco, C. 2007, *MNRAS*, 374, 323
- Edmunds, M. G. 1990, *MNRAS*, 246, 678
- Ellison, S. L. & Kewley, L. J. 2005, in proc. "The Fabulous Destiny of Galaxies; Bridging the Past and Present", *astro-ph/0508627*
- Erb, D. K., Shapley, A. E., Pettini, M., Steidel, C. C., Reddy, N. A., & Adelberger, K. L. 2006, *ApJ*, 644, 813
- Finlator, K., Davé, R., Papovich, C., & Hernquist, L. 2006, *ApJ*, 639, 672
- Finlator, K., Davé, R., & Oppenheimer, B. D. 2007, *MNRAS*, 376, 1861
- Garnett, D. R., Shields, G. A., Skillman, E. D., Sagan, S. P., & Dufour, R. J. 1997, *ApJ*, 489, 63
- Garnett, D. R. 2002, *ApJ*, 581, 1019
- Geha, M., Blanton, M. R., Masjedi, M., & West, A. A. 2006, *ApJ*, 653, 240
- Guo, Q., & White, S. D. M. 2007, *ArXiv e-prints*, 708, *arXiv:0708.1814*
- Haardt, F. & Madau, P. 2001, in proc. XXXVIth Rencontres de Moriond, eds. D.M. Neumann & J.T.T. Van.
- Heckman, T. M. 2003, *Revista Mexicana de Astronomia y Astrofisica Conference Series*, 17, 47
- Iglesias-Paramo, J., et al. 2007, *ArXiv e-prints*, 707, *arXiv:0707.3415*
- Kauffmann, G., White, S. D. M., Heckman, T. M., Ménard, B., Brinchmann, J., Charlot, S., Tremonti, C., & Brinkmann, J. 2004, *MNRAS*, 353, 713
- Kennicutt, R. C. 1998, *ApJ*, 498, 541
- Kereš, D., Katz, N., Weinberg, D. H., & Davé, R. 2005, *MNRAS*, 363, 2
- Kobayashi, C., Springel, V., & White, S. D. M. 2007, *MNRAS*, 376, 1465
- Köppen, J., & Edmunds, M. G. 1999, *MNRAS*, 306, 317
- Köppen, J., & Hensler, G. 2005, *AAP*, 434, 531
- Köppen, J., Weidner, C., & Kroupa, P. 2007, *MNRAS*, 375, 673
- Kovac, K., et al. 2007, *ApJ*, submitted
- Larson, R. B. 1972, *Nature*, 236, 7
- Larson, R. B. 1974, *MNRAS*, 169, 229
- Lee, H., Skillman, E. D., Cannon, J. M., Jackson, D. C., Gehrz, R. D., Polomski, E. F., & Woodward, C. E. 2006, *ApJ*, 647, 970
- Lequeux, J., Peimbert, M., Rayo, J. F., Serrano, A., & Torres-Peimbert, S. 1979, *AAP*, 80, 155
- Mathews, W. G., & Baker, J. C. 1971, *ApJ*, 170, 241
- Mac Low, M.-M., & Ferrara, A. 1999, *ApJ*, 513, 142
- Martin, C. L. 1999, *ApJ*, 513, 156
- Martin, C. L. 2005, *ApJ*, 621, 227
- McClure, R. D., & van den Bergh, S. 1968, *AJ*, 73, 1008
- McKee, C. F. & Ostriker, J. P. 1977, *ApJ*, 218, 148
- Murray, N., Quatert, E., & Thompson, T. A. 2005, *ApJ*, 618, 569
- Neistein, E., van den Bosch, F. C., & Dekel, A. 2006, *MNRAS*, 372, 933
- Noeske, K. G., et al. 2007, *ApJL*, 660, L43
- Noeske, K. G., et al. 2007, *ApJL*, 660, L47
- Oppenheimer, B. D., & Davé, R. 2006, *MNRAS*, 1268
- Pilyugin, L. S. Vílchez, J. M., & Contini, T. 2004, *AAP*, 425, 849
- Portinari, L., Chiosi, C., & Bressan, A. 1998, *A&A*, 334, 505
- Rix, S. A., Pettini, M., Leitherer, C., Bresolin, F., Kudritzki, R.-P., & Steidel, C. C. 2004, *ApJ*, 615, 98
- Rupke, D. S., Veilleux, S., & Sanders, D. B. 2005, *ApJS*, 160, 115
- Salpeter, E. E. 1955, *ApJ*, 121, 161
- Savaglio, S., et al. 2005, *ApJ*, 635, 260
- Scannapieco, E., & Broadhurst, T. 2001, *ApJ*, 549, 28
- Schaerer, D. 2003, *AAP*, 397, 527
- Shapley, A. E., Coil, A. L., Ma, C.-P., & Bundy, K. 2005, *ApJ*, 635, 1006
- Somerville, R. S., Primack, J. R., & Faber, S. M. 2001, *MNRAS*, 320, 504
- Songaila, A. 2001, *ApJL*, 561, L153
- D. N. Spergel *et al.*, *ApJS*, 148, 175
- Springel, V. & Hernquist, L. 2002, *MNRAS*, 333, 649
- Springel, V. & Hernquist, L. 2003a, *MNRAS*, 339, 289
- Springel, V. & Hernquist, L. 2003b, *MNRAS*, 339, 312
- Straughn, A. N., Cohen, S. H., Ryan, R. E., Hathi, N. P., Windhorst, R. A., & Jansen, R. A. 2006, *ApJ*, 639, 724
- Sutherland, R. S. & Dopita, M. A. 1993, *ApJS*, 88, 253
- Tassis, K., Kravtsov, A. V., & Gnedin, N. Y., *ApJ* submitted, *astro-ph/0609763*
- Tinsley, B. M. 1980, *Fundamentals of Cosmic Physics*, 5, 287
- Tinsley, B. M., & Larson, R. B. 1978, *ApJS*, 221, 554
- Tremonti, C. A., Heckman, T. M., Kauffmann, G., et al. 2004, *ApJ*, 613, 898
- Weinberg, D. H., Davé, R., Gardner, J. P., Hernquist, L., & Katz, N. 1999, in "Photometric Redshifts and High Red-

- shift Galaxies”, eds. R. Weymann, L. Storrie-Lombardi, M. Sawicki & R. Brunner, (San Francisco: ASP Conf. Series v.191), p.341
- Woosley, S. E., & Weaver, T. A. 1995, *ApJS*, 101, 181
- Zaritsky, D., Kennicutt, R. C., Jr., & Huchra, J. P. 1994, *ApJ*, 420, 87
- Zheng, X. Z., Bell, E. F., Papovich, C., Wolf, C., Meisenheimer, K., Rix, H.-W., Rieke, G. H., & Somerville, R. 2007, *ApJL*, 661, L41